Interactome and structural basis for targeting the human T-cell leukemia virus Tax oncoprotein

Sibusiso B. Maseko[1], Inge Van Molle[2], Karim Blibek[1], Christoph Gorgulla[3-5], Julien Olivet[1], Jeremy Blavier[1], Charlotte Vandermeulen[1], Stéphanie Skupiewski[1], Deeya Saha[1], Thandokuhle Ntombela[6], Julianne Lim[7], Frederique Lembo[8], Aurelie Beauvois[9], Malik Hamaidia[9], Jean-Paul Borg[8], Pascale Zimmermann[8,10], Frank Delvigne[11], Luc Willems[9,11], Johan Van Weyenbergh[12], Dae-Kyum Kim[7, 13-15], Franck Dequiedt[16], Haribabu Arthanari[3-5], Alexander N. Volkov[2,17,*], Jean-Claude Twizere[1,11,18,*]

[1]Laboratory of Viral Interactomes, Unit of Molecular Biology of Diseases, GIGA Institute, University of Liege, Liège, Belgium. [2]VIB-VUB Center for Structural Biology, Flemish Institute of Biotechnology (VIB), Pleinlaan 2, Brussels, Belgium. [3]Department of Biological Chemistry and Molecular Pharmacology, Blavatnik Institute, Harvard Medical School, Boston, MA, USA. [4]Department of Physics, Faculty of Arts and Sciences, Harvard University, Cambridge, MA, USA. [5]Department of Cancer Biology, Dana-Farber Cancer Institute, Boston, MA, USA. [6]Catalysis and Peptide Research Unit, School of Health Sciences, University of KwaZulu Natal, Durban 4001, South Africa. [7]Center for Personalized Medicine, Roswell Park Comprehensive Cancer Center, Buffalo, New York, USA. [8]Aix Marseille Univ, CNRS, INSERM, Institut Paoli-Calmettes, CRCM, Equipe labellisée Ligue 'Cell polarity, Cell signaling and Cancer, Marseille, France. [9]Laboratory of Cellular and Molecular Epigenetics, Cancer Unit, GIGA Institute, University of Liege, Liege, Belgium. [10]Department of Human Genetics, KU Leuven, Belgium. [11]TERRA research and teaching centre, Microbial Processes and Interactions (MiPI), Gembloux Agro Bio-tech, University of Liege. [12]Laboratory of Clinical and Epidemiological Virology, Rega Institute for Medical Research, Department of Microbiology. [13]The Donnelly Centre, University of Toronto, Toronto, ON, Canada. [14]Department of Molecular Genetics, University of Toronto, Toronto, ON, Canada. [15]Lunenfeld Tanenbaum Research Institute, Mount Sinai Hospital, Toronto, ON, Canada. [16]Laboratory of Gene Expression and Cancer, Molecular Biology of Diseases Unit, GIGA Institute, University of Liege, Liege, Belgium. [17]Jean Jeener NMR Centre, Free University of Brussels (VUB), Pleinlaan 2, Brussels Belgium
[18]Lead contact

*Correspondence: Oleksandr.Volkov@vub.be (A.N.V.), jean-claude.twizere@uliege.be (JC.T.)

SUMMARY

Human T-cell leukemia virus type-1 (HTLV-1) is the first pathogenic retrovirus discovered in human. Although HTLV-1-induced diseases are well characterized and linked to the encoded Tax-1 protein, there is currently no strategy to target Tax-1 functions with small molecules. Here, we report a comprehensive interaction map between Tax-1 and human PDZ domain-containing proteins (hPDZome), and we show that Tax-1 interacts with one-third of them. This includes proteins involved in cell cycle, cell-cell junction and cytoskeleton organization, as well as in membrane complexes assembly. Using nuclear magnetic resonance (NMR) spectroscopy, we have determined the structural basis of the interaction between the C-terminal PDZ binding motif (PBM) of Tax-1, and the PDZ domains of DLG1 and syntenin-1. Finally, we have used molecular modeling and mammalian cell-based assays to demonstrate that Tax-1/PDZ-domain interactions are amenable to small-molecule inhibition. Thus, our work provides a framework for the design of targeted therapies for HTLV-1-induced diseases.

Highlights

- A comprehensive interactome map of HTLV-1 Tax / human PDZ proteins
- Structural basis of Tax-1 PBM binding to human DLG1 and syntenin-1 PDZ domains".
- Biological significance of inhibiting Tax-1 functions
- Druggability of the Tax-1 / PDZ interface

Graphical abstract

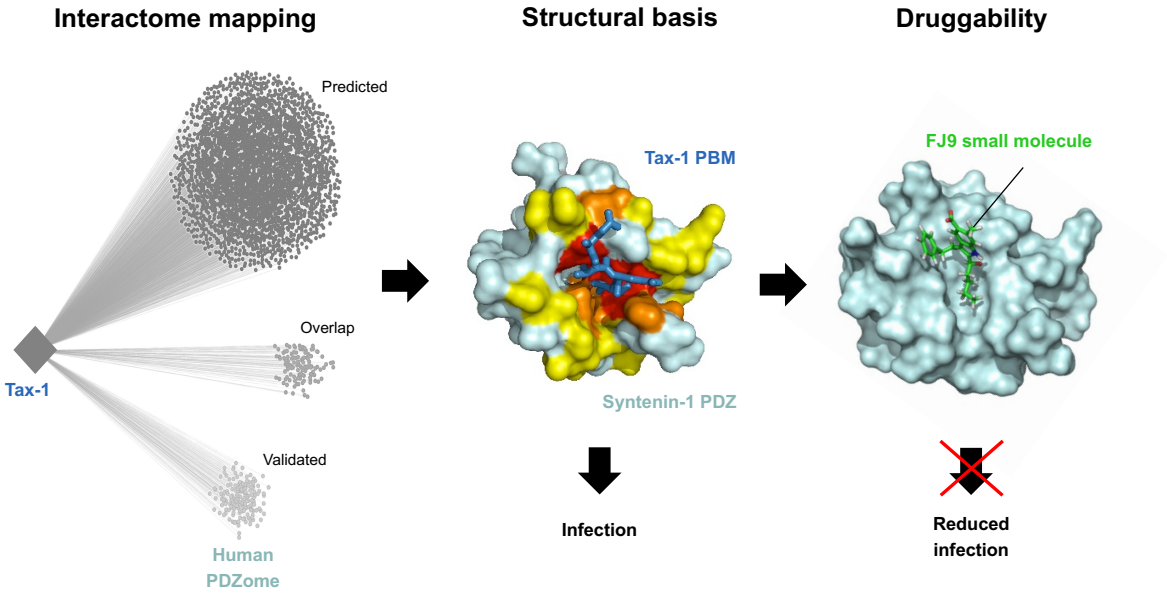

INTRODUCTION

Human T-cell lymphotropic viruses (HTLV-1 to -4) are members of *Deltaretrovirus* genus of the *Retroviridae* family. The first human retrovirus to be isolated 40 years ago (Poiesz et al., 1981), HTLV-1 is the etiological agent of adult T-cell leukemia/lymphoma (ATL), an aggressive neoplasm, as well as HTLV-1-associated myelopathy (HAM). HAM is also termed tropical spastic paraparesis (TSP) (HAM/TSP), an immune degenerative neurologic syndrome. HTLV-2 was discovered shortly after HTLV-1 (Kalyanaraman et al., 1982), but has not been convincingly linked to lymphoproliferative disorders (Feuer and Green, 2005). HTLV-3 and 4 were the latest identified (Calattini et al., 2005; Wolfe et al., 2005), and their possible association with human diseases needs further investigation. Currently about 10-20 million people worldwide are infected with HTLV-1, and 1 to 10% will develop severe ATL or HAM/TSP diseases (Gessain et al., 1985; Hinuma et al., 1981; Pasquier et al., 2018). For the last 40 years, ATL patients have been treated using chemotherapy-based approaches, but with very limited benefit the median survival rate being 8-10 months (Bazarbachi et al., 2011; Cook and Phillips, 2021; Utsunomiya et al., 2015). Improved survival is achieved by antiviral therapies combining zidovudine and interferon-alpha (Nasr et al., 2017), allogenic hematopoietic stem cell transplantation (Fuji et al., 2016), or the use of monoclonal antibodies targeting CC chemokine receptor 4 (CCR4), which is frequently expressed in ATL patient samples (Ishida et al., 2015; Yoshie, 2005; Yoshie et al., 2002). However, the above therapies are not fully effective, mainly due to clinical disease heterogeneity, discrepancies in treatment between countries, and lack of specific and universally targeted drugs (Cook and Phillips, 2021). In contrast to ATL, no treatment is available for HAM/TSP patients. Both HTLV-1-induced diseases are associated with high proviral loads. Targeting viral replication, including re-positioning existing anti-human immunodeficiency virus (HIV) drugs, was investigated to decrease HTLV-1 cell-to-cell transmission (Pasquier et al., 2018) and may lead to effective anti-HTLV-1 therapies.

In addition to the essential retroviral genes *gag*, *pol* and *env*, HTLV-1 encodes regulatory proteins including Tax-1, Rex, p12I, p13II, p30II and HBZ. The Tax-1 protein is a major determinant in HTLV pathogenesis and persistence. The transforming activity of HTLV-1 has been essentially attributed to the *Tax-1* gene, which is able to induce leukemia-lymphoma in transgenic mice (Hasegawa et al., 2006; Ohsugi et al., 2007). The Tax-1 protein is indeed a potent transcriptional activator of viral and cellular genes through association with transcription modulators including CREB (Ohsugi *et al.,* 2007) ,SRF (FuJil et al., 1988; Winter and Marriott, 2007) , AP-1 (Yoshida, 2001), NF-kB (Ballard et al., 1988; Béraud et al., 1994; Leung and Nabel, 1988; Xiao et al., 2001), CBP/p300 (Harrod et al., 1998; Kwok et al., 1996), PCAF (Jiang et al., 1999), and P-TEFb (Cho et al., 2010). Thus, Tax-1 deregulates an array of cellular genes directly involved in T-cell proliferation (Albrecht et al., 1992; Crenon et al., 1993; Himes et al., 1993; Maruyama et al., 1987; Twizere et al., 2003), migration (Twizere et al., 2007), apoptosis (Taylor and Nicot, 2008), and cell-cycle (Neuveut and Jeang, 2000; 2002).

Tax-1 is a multidomain protein harboring intrinsically disordered linker regions, encompassing residues 76 - 121, 252 - 275, and the C-terminal amino acids 320 -353 (Boxus et al., 2008). Such modular organization ensures conformational plasticity and could explain dynamic hijacking of crucial cellular functions through interaction with a variety of targets. More than 200 cellular proteins have been reported to interact with Tax (Boxus *et al.*, 2008; Legros et al., 2009; Simonis et al., 2012a), including numerous signaling molecules such as IκB kinases (Harhaj and Sun, 1999; Jin et al., 1999), MAPK/ERK kinase 1 (MEKK1) (Yin et al., 1998), TGF-beta activating kinase 1 (TAK1) (Wu and Sun, 2007), c-Jun N-terminal kinase 1 (JNK), phosphatidylinositol 3-kinase and its downstream messenger protein kinase B (Liu et al., 2001; Peloponese Jr and Jeang, 2006), protein phosphatases (Hong et al., 2007), GTP-binding proteins (Twizere *et al.*, 2007; Wu et al., 2004), cytoskeleton components (Nejmeddine et al., 2005; Wu *et al.*, 2004), cell cycle molecules (Haller et al., 2000; Haller et al., 2002; Kehn et al., 2005; Kehn et al., 2004), nuclear effectors such as histone and chromatin modifier enzymes (Kamoi et al., 2006; Legros et

al., 2011), and mini-chromosome maintenance proteins (Boxus et al., 2012). The carboxyl terminus of Tax-1 harbors a PDZ-binding motif (PBM), which confers binding to a class of proteins containing a defined structure of ~90 amino acids known as PDZ (PSD-95/Discs Large/ZO-1) domain (Sheng and Sala, 2001; Tonikian et al., 2008b). PDZ-containing proteins are modular polypeptides implicated in large protein complexes assembly, mediating signaling, cell polarity, and communication (Hung and Sheng, 2002). Our analysis of the human genome estimates the presence of 256 PDZ domains in 149 distinct proteins, excluding variants and isoforms (Belotti et al., 2013a). To date, 14 PDZ proteins interacting with HTLV-1 Tax have been identified (Boxus *et al.*, 2008; Yan et al., 2009). Tax-1-PDZ protein interactions have important implications in HTLV-1-induced leukemogenesis process. In particular, it was shown that the Tax-1 PBM motif, which is not present in the HTLV-2 Tax counterpart, promotes transformation of rat fibroblasts and mouse lymphocytes *in vitro* (Higuchi et al., 2007; Hirata et al., 2004a; Tsubata et al., 2005), as well as persistence of the HTLV-1 virus *in vivo* (Xie et al., 2006).

In this study, we hypothesized that targeting Tax-1-PDZ interactions would provide novel anti-HTLV-1 transmission strategies, which could potentially be used to combat ATL and TSP/HAM diseases. We therefore comprehensively mapped the Tax-1 interactome with human PDZ-containing proteins and found that about one third of the human PDZome is capable of specific interactions with Tax-1. Using nuclear magnetic resonance (NMR) spectroscopy, we structurally characterized interactions between Tax-1 PBM and PDZ domains from two highly relevant host proteins, the human homolog of the drosophila discs large tumor suppressor (DLG1/SAP97) and syntenin-1. Finally, we demonstrate that FJ9, a small molecule able to disrupt Tax-1-syntenin-1 interaction, inhibits several Tax-1 functions, including cell immortalization and HTLV-1 cell-to-cell transmission.

RESULTS

A comprehensive interactome map of Tax-1 with human PDZ-containing proteins

The *Tax-1* viral oncogene is a hallmark of initiation and maintenance of HTLV-1-induced diseases. However, the encoded Tax-1 protein is still viewed as "undruggable", essentially because of its pleiotropic effects on cellular systems and low expression levels in most HTLV-1-infected cells. We reasoned that a detailed understanding of the Tax-1 interactome could reveal druggable Tax-1 interactome modules, amenable to small molecule inhibition. We have previously highlighted the function of Tax as a *"hub"* molecule, capable of interacting with several host cell complexes modules at the transcription, post-transcription, and translation levels (Simonis et al., 2012b; Vandermeulen et al., 2021). To date, high throughput and small-scale focused studies identified 258 human proteins interacting with Tax-1 (Vandermeulen *et al.*, 2021). To comprehensively estimate the size of the Tax-1 interactome, we identified Tax targets based on motif-domain and domain-domain interactions and predicted 2401 human proteins, including 161 experimentally validated partners, as potential targets for Tax (Figure 1A). This suggests that about 10% of the full human proteome could be affected by this viral oncoprotein through a well-defined set of protein modules (Table S1).

In order to understand the functional plasticity of the Tax interactome, we hypothesized that transient associations controlled by multi-domain scaffolding proteins are able to dynamically relocate Tax complexomes within the cell, as recently demonstrated for binary interactome yeast models (Lambourne et al., 2021). In the context of Tax-1, human PDZ-containing proteins appear as the best candidates connecting Tax-1 and host protein complexes located in different cellular compartments. To generate a complete interactome of Tax-1 with human PDZ-containing proteins, we combined three different sources of Tax-1 protein-protein interaction (PPI) datasets (Figures 1B and S1A): (i) literature-

curated high quality interactions (Figure S1B); (ii) systematic yeast two hybrid interactions obtained by testing a library of 248 individualized PDZ domains, orthogonally validated using Gaussia princeps luciferase complementation (GPCA) assay (Cassonnet et al., 2011); and (iii) GST-pulldown analyses of open reading frames (ORFs) available in the human ORFeome collections (http://horfdb.dfci.harvard.edu/hv7/) (Figures S1C-D). Our map of the Tax-PDZ interactome (Figure 1B) contains 56 human proteins, representing 37% of the human PDZome (Belotti et al., 2013b), and a substantial increase from the 14 already known human PDZ proteins directly interacting with Tax (Figure S1B).

To further determine the relative implication of PDZ-containing proteins in the human interactome, we used our recently released human binary reference interactome map (HuRI) (Luck et al., 2020), and ranked PDZ proteins according to the number of their direct interactors (" first degree") or indirect associations ("second degree") (Table S2). The average first and second degrees of Tax-1 partners were 24 and 536 PPIs, respectively, further emphasizing the scaffolding role of PDZ-containing proteins targeted by the viral Tax oncoprotein.

To assess the overall biological significance of Tax-PDZ interactome, we investigated the expression of human PDZ protein coding genes in different relevant datasets: (i) expression data across 24 different T-cell lines (Figure 1C); (ii) differential expression data in HTLV-1-infected versus non-infected cells (Figure 1D); (iii) differential expression data in Jurkat cells expressing Tax-1 versus control cells (Figure 1E); (iv) mutational landscapes in ATL patient samples (Figure 1F); and (v) transcriptome data from a "gene signature" of ATL (Bazarbachi, 2016; Fujikawa et al., 2016) (Figure 1G). Finally, we performed spatial analysis of functional enrichment (SAFE) (Baryshnikova, 2016) using the above datasets and a STRING network of Tax-1/PDZ interactors (Table S2). We identified five functional modules including nucleic acid binding, nuclear ubiquitin binding, regulation of cell cycle, cell-cell junction and cytoskeleton organization, and endocytic vesicles membrane assembly (Figure 1H). Thus, it appears that the described Tax-1/PDZ interactome

is implicated in various Tax functions, from early steps of T-cell infection by HTLV-1 to subsequent disease progression.

The structural basis of Tax/ hDLG1 PDZ interactions

To characterize the Tax-1-PDZ interactions at the molecular level, we first addressed the association between Tax-1 and the human homolog of the drosophila discs large tumor suppressor (hDLG1/SAP97). hDLG1 is the first PDZ-containing protein identified to interact with Tax-1 and other viral oncoproteins such as HPV 18 E6 and adenovirus E4-ORF1 (Lee et al., 1997). While the Tax-1-hDLG1 binding detailed here (Figures S2A-B) was also functionally validated by numerous previous studies (Aoyagi et al., 2010; Hirata et al., 2004b; Marziali et al., 2017; Suzuki et al., 1999), its structural basis remained unknown.

To obtain molecular-level details of Tax-1-hDLG1 interaction, we employed solution nuclear magnetic resonance (NMR) spectroscopy. First, we studied binding of the last 10 C-terminal amino acids of Tax-1 (Tax-1 10mer peptide: SEKHFRETEV) to the tandem PDZ1+2 domains of hDLG1. Monitored in a series of [^{1}H,^{15}N] heteronuclear single-quantum correlation (HSQC) experiments, binding of the natural-abundance, NMR-silent Tax-1 10mer to the ^{15}N labeled, NMR-visible hDLG1 PDZ1+2 leads to large spectral changes (Figures 2A-B). When titrated with Tax-1 10mer, the HSQC peaks of ^{15}N hDLG1 PDZ1+2 progressively disappear and then reappear elsewhere in the spectrum at the end of the titration, a behavior symptomatic of the slow exchange NMR regime (Figure 2A). For both PDZ domains, the strongest effects are observed for the residues in and around the canonical peptide binding site, formed by the β1/β2 loop, the β2 strand and the α2 helix (Figure 2B). In particular, the largest binding shifts are detected for the PBM residues G235 and F236 of PDZ1 and G330 and F331 of PDZ2 (Figures 2A-B). The resulting chemical shift perturbation maps illustrate the contiguous protein surfaces of both PDZ1 and PDZ2 targeted by the Tax-1 10mer peptide (Figures 2C-D).

To investigate whether individual hDLG1 PDZ domains function as independent modules, we expressed and purified single PDZ domains (Figure S2A) and probed their Tax-1 binding properties by NMR spectroscopy. Overall, the binding effects of Tax-1 10mer to PDZ1 (Figures 2E-H) or PDZ2 (Figures 2I-L) domains are similar to those observed for the PDZ1+2 tandem (Figures 2A-D). The interaction of Tax-1 10mer with PDZ2 is stronger than that with PDZ1 (K_D of 0.9 μM and 2.7 μM, respectively; Figures 2H, L), which is in agreement with our GST-pulldown assay using a Tax-1 protein from HTLV-1 producing MT2 cells (Figure S2B).

To narrow down further the Tax-1 binding requirements, we performed NMR experiments with the peptides corresponding to the last four and first six amino acids of the Tax-1 10mer. The C-terminal PBM fragment (ETEV) interacts with the ^{15}N hDLG1 PDZ1+2 tandem in the same way as the Tax-1 10mer (Figures S3A-D), while no binding of the N-terminal 6mer peptide (SEKHFR) could be observed (Figures S4A-B). These findings demonstrate that the four C-terminal residues of Tax-1, bearing the X-S/T-X-V binding motif, are necessary and sufficient for the interaction with the hDLG1 PDZ1 and PDZ2 domains. This interaction also requires a free C-terminal carboxyl group of Tax-1 as illustrated by smaller chemical shift perturbations and a 360-fold decrease of the binding affinity in NMR experiments with a chemically modified, C-terminally amidated peptide (Figures S4C-F).

Finally, to assess the binding specificity, we performed NMR experiments with a peptide corresponding to the last 10 amino acids of Tax-2 (NKEEADDNGD), encoded by another member of Deltaretroviruses, the HTLV-2 virus, which is not leukemogenic in human (Martinez et al., 2019). Tax-2 protein has several structural similarities with Tax-1 but does not contain a PBM at its C-terminus. Compared to Tax-1 10mer (Figure 2A), the interaction of the C-terminal Tax2 10mer peptide with ^{15}N hDLG1 PDZ1+2 tandem does not induce binding shifts of residues G235, F236, G330, or F331 (Figures S2C-D). Instead, it leads to chemical shift perturbations for several residues in discontinuous

patches at the side and the back of the protein, outside the canonical peptide binding sites (Figure S2E). Stepwise addition of Tax2 10mer to ^{15}N hDLG1 PDZ1+2 results in incremental shifts for some of the backbone amide resonances, a behavior typical for the NMR fast exchange regime. The resulting binding curves are very shallow and do not saturate even at the 10-fold molar excess of the added peptide (Figure S2F), suggesting a very weak interaction (KD > 5 mM). Overall, the very weak binding to several protein regions outside the canonical peptide binding sites suggests that the interaction of Tax2 10mer with the hDLG1 PDZ1+2 tandem is aspecific.

A crosstalk between Tax-1-PDZ interaction and membrane vesicles trafficking

The above SAFE analysis highlighted endocytic vesicles membrane assembly as one of the enriched functions in the Tax-1/PDZ interactome (Figure 1G). The subnetwork of this function highlights syndecan binding protein 1 (SDCBP1 also known as syntenin-1), which has the highest connectivity in this subnetwork (Figure 3A) and also in our recently released human interactome map (Luck *et al.*, 2020) (HuRI), http://www. interactome-atlas.org/). Syntenin-1 is particularly relevant for viral infections as it controls extracellular vehicles (EVs, also called exosomes) formation and cell-to-cell communication (Imjeti and Menck, 2017; Kim et al., 2015). A direct interaction between syntenin-1 and programmed cell death 6 interacting protein (PDCD6IP also called ALG-3 interacting protein X (ALIX) (Christ et al., 2016), was demonstrated and provided fundamental insights on the interplay between exosomes formation and the endosomal sorting complexes for transport (ESCRT) pathway (Baietti et al., 2012). ALIX and other components of the ESCRT pathway are recruited by structural proteins of enveloped viruses to facilitate budding (Göttlinger et al., 1991; Hanson and Cashikar, 2012; Votteler and Sundquist, 2013). Importantly, Tax-1, which is a regulator protein, has been shown to localize into EVs from HTLV-1 infected cells. These Tax-1-containing exosomes significantly contribute to viral spread and disease progression (Al Sharif et al., 2020; Pinto et al., 2019). However, the molecular mechanisms controlling Tax-1 recruitment into EVs are unknown. We therefore tested the possibility that syntenin-1 could mediate Tax-1 localization into exosomes. As shown in Figure 3B, a siRNA targeting syntenin-1 expression is associated with a

reduction of the Tax-1 amount in exosomes, in accordance with Tax-1 translocation from the cytoplasm to the nucleus (Figure 3C). These findings suggest that syntenin-1 is required for Tax-1 translocation into EVs. We have extensively characterized the Tax-1/syntenin-1 interaction, as well as the interaction between Tax-1 and syntenin-2, using yeast two hybrid (Figure 3D), co-immunoprecipitations (Figure 3E), and GST-pulldown assays (Figure 3F). It appears that both syntenin proteins interact with Tax-1, but not with HTLV-2 Tax lacking a PBM, further demonstrating the specificity of Tax-1 PBM for syntenin PDZ domains. Thus, thanks to its PDZ domains, syntenin-1 can act as a molecular bridge, targeting Tax-1 to EVs via the ESCRT pathway.

The structural basis of Tax/ syntenin-1 PDZ interactions

To determine the structural basis of Tax-1/syntenin-1 interaction, we employed solution NMR spectroscopy using natural abundance Tax-1 10mer and isotopically labelled PDZ1, PDZ2 and tandem PDZ1+2 syntenin-1 domains (Figure 4A). Addition of Tax-1 10mer to ^{15}N syntenin-1 PDZ1+2 leads to incremental chemical shift changes for some of the resonances, several of which progressively disappear in the course of the titration, which is symptomatic of the fast-to-intermediate NMR exchange regime. The chemical shift perturbations map onto the canonical peptide binding sites of both PDZ1 (residues I125 and G126) and PDZ2 (residues V209, G210, F211 and F213) domains, encompassing the β1/β2 loop, the β2 strand, and the α2 helix (Figure 4A). The binding effects are stronger for the PDZ2 domain and appear to extend to the back of the protein (residues T200, L232 and T266) (Figure 4B). These findings are consistent with an earlier study of syntenin-1-peptide interactions by X-ray crystallography that highlighted a binding-induced reorientation of the α2 helix(Grembecka et al., 2006a), which could explain the chemical shift perturbations of the residues at the back of PDZ2 (Figure 4B). As for hDLG1 PDZ1+2 tandem, NMR experiments with the Tax-1 PBM 4mer and the control Nter 6mer peptides illustrate that, the four C-terminal residues of Tax-1 (ETEV) are necessary and sufficient for the interaction with the syntenin-1 PDZ1 and PDZ2 domains (Figures S5).

To evaluate the binding contribution of each PDZ domain, we performed NMR experiments with Tax-1 10mer and individually expressed syntenin-1 PDZ1 and PDZ2 domains. The chemical shift perturbation maps for isolated PDZ1 (Figures 4C-4E) and PDZ2 (Figures 4F-H) are similar to those for the PDZ1+2 tandem (Figures 4A-B). As for hDlG1, a slight preference for the PDZ2 domain is observed, with K_Ds of 2.6 and 1. 6 mM for PDZ1 and PDZ2, respectively (Figures 4E,4H).

A small molecule inhibitor of Tax-1-syntenin-1 interactions

To determine the extent to which small molecules could interfere with Tax functions via inhibition of Tax-1/PDZ interactions, we used FJ9 (Figure 5A), a previously characterized small molecule inhibitor (Fujii et al., 2007). FJ9 was able to suppress β-catenin-dependent tumor cell growth in a mouse model, following perturbation of the interaction between the Wnt receptor Frizzled-7 (Frz7) and Dishevelled Segment Protein 3 (DVL3), a PDZ-containing protein overexpressed in several cancer cells (Fujii *et al.*, 2007). Inhibition of Wnt-β-catenin signaling pathway was also shown to induce cell death in ATL and HTLV-1 transformed cell lines (Ying and Tao, 2009). To examine whether FJ9 could also disrupt the Tax-1/PDZ binding, we sought to investigate the FJ9 interaction with syntenin-1 PDZ domains. Unfortunately, the low FJ9 solubility in aqueous buffers precluded the binding analysis by NMR spectroscopy or other biophysical techniques. However, we have successfully performed an *in silico* molecular docking, which showed that FJ9 engages the canonical peptide binding site of syntenin-1 PDZ2 (Figure 5B). The FJ9 molecule makes extensive intermolecular contacts, including hydrophobic interactions with syntenin -1 residues V209, F211, I212, and F213 and a hydrogen bond with the backbone carbonyl atom of F211 (Figure 5B). Interestingly, these are the key residues mediating the Tax-1/syntenin-1 interaction (Figures 4A-B), suggesting that FJ9 competes with Tax-1 PBM for the binding to syntenin-1 PDZ domains.

We next employed YFP-based bimolecular fluorescence complementation (BiFC) assay, which provides direct visualization and quantification of protein interactions in living cells (Hu et al., 2002). We fused the two YFP-BiFC fragments to the N- and C-terminal ends

of Tax-1 and syntenin coding sequences, respectively. Pairs of fusion proteins were expressed in HEK293 cells, and fluorescent complementation was quantified by flow cytometry. As shown in Figures 5C-D, interaction between Tax-1 and syntenin-2 exhibited the highest rate of complementation (33%), compared to Tax-1 and syntenin-1 (14%). This finding is consistent with our co-immunoprecipitation, pulldown, and co-localization assays showing stronger interactions with syntenin-2 (Figures 3E-G). To determine whether the small molecule FJ9 could disrupt the Tax-1/syntenin interaction, HEK 293 cells transfected with Tax-1/syntenin-1 or Tax-1/syntenin-2 pairs of YFP-BiFC fused constructs were treated with 300 µM of FJ9 for 24h. The FJ9 treatment drastically diminished the rate of fluorescence complementation (33% to 4% for Tax-1/syntenin-2 and from 14% to 2,6% for Tax-1/syntenin-1) (Figures 5C-D) . We therefore conclude that FJ9 efficiently disrupts Tax/syntenin complex formation in cells.

The Tax-1 PBM has been shown to increase its oncogenic capacity in cell culture (Higuchi *et al.*, 2007). To examine whether FJ9 could inhibit the Tax-transformation activity, we infected a rat fibroblast cell line (Rat-1) with a VSV-G packaged lentiviral construct harboring the HTLV-1 tax gene and the blasticidin resistant gene (CS-EF-IB-Tax-1). Cells were selected by blasticidin, and pools of resistant cells seeded for a colony formation in soft agar assay (CFSA) in the presence or absence of FJ9 (100 µM). As shown in Figure 5E, HTLV-1 Tax transformed Rat-1 cells form multiple large colonies in CFSA, as previously described (Higuchi *et al.*, 2007). In the presence of FJ9, Rat-1 cells formed much smaller colonies, and their number was reduced compared to the cells treated with the vehicle. Thus, we conclude that FJ9 inhibits Tax-transformation activity in the Rat-1 model (Figures 5E-F).

To probe the role of the Tax/PDZ interaction in cell-to-cell HTLV-1 transmission, we performed a co-culture experiment using Jurkat T-cell line reporter expressing luciferase under the control of the 5'LTR HTLV-1 promoter, and an HTLV-1 producing cell line (MT2) or as negative control, a human T cell leukemia cell line (CEM) Figure 5G). The reporter exhibits basal levels of luciferase expression, which increase following co-culture with

MT2 cells and transactivation of the 5'LTR by Tax. We showed that at 100 µM, a dose which does not induce significant cell death compared to the vehicle (Figure 5H), FJ9 was able to inhibit HTLV-1 transmission, reducing Tax transactivation to the basal level (Figure 5I).

DISCUSSION

Host factors as antiviral targets

Despite the discovery of viruses in the early 1900s, and the demonstration of their pathogenicity in humans in early 1950s, the arsenal of antiviral drugs remains dangerously small, with only ~90 molecules available today (De Clercq and Li, 2016). Those are biased towards viral enzymes, including polymerases, proteases, and integrases. Furthermore, 95% of approved drugs target only 6 types of viruses (HIV-1, HCV, HBV, HSV, HCMV, and Influenza viruses), with HIV-1 covering the majority of available drugs. As evidenced by the current coronavirus disease 19 (COVID19) pandemic, it is of utmost importance to anticipate emerging and re-emerging viral infections by identifying potential broad-spectrum antiviral drugs. However, this task is rendered difficult by many formidable challenges, among which are (i) the druggability of viral products, (ii) the antiviral drug safety, and (iii) a desirable high potency to limit the selection of resistant mutations. High-throughput mapping of host-virus PPIs and massively parallel genomic sequencing have accelerated the pace of discovery of key host targets, which are shared by different categories of pathogenic viruses, including RNA and DNA, or acute and persistent viruses (Rozenblatt-Rosen et al., 2012; Tang et al., 2013; Watanabe et al., 2014). These host factors provide novel opportunities to prioritize antiviral drugs based on common host targets. In this work, our goal was to demonstrate that one of such host determinants, the PDZ-domain containing proteins, could provide insights into how to identify small molecule inhibitors of viral-host PPIs.

Towards a virus-host-omes/chemo-interactomics pipeline

The methodology used here defines a pipeline that could be applied to any pathogenic parasite of interest, without prior knowledge on the druggability of its encoded gene products. First, we chose HTLV-1 Tax (Tax-1), a highly connected viral oncoprotein, and demonstrated that it has the potential to interact with 10% of the human proteome through defined interactome modules. Second, we systematically mapped the interactome of Tax-1 with one of its cellular modules, the PDZ domain, and assessed the biological significance of that particular portion of the Tax interactome by integrating expression and genomic data from HTLV-1-infected patients. Third, we determined the structural basis of Tax-1 C-terminal motif binding to canonical sites of hDLG1 and syntenin-1 PDZ domains. Finally, we demonstrated that a small molecule targeting Tax-1-syntenin interactions could inhibit Tax-1 functions in cellular models.

Host targets prioritization

By testing 248 out of 268 PDZ domains identified in 151 human proteins, our results establish the first comprehensive Tax-1-PDZ interactome, highlighting a set of 54 PDZ- domain containing proteins. Comparative analyses with similar unbiased mapping for other viral proteins are now possible. For example, hDLG1 and SCRIB have also been shown to interact with HPV E6, Ad9 E4orf1, IAV NS1, HTLV-1 Env, HIV-1 Env and HCV core proteins, but with different biological outcomes, including perturbations of cell polarity, signaling, or apoptosis (Thomas and Banks, 2018). Interestingly, the conserved C-terminal PBM motifs of these viral proteins highly correlate with viral pathogenicity, independently of their substantial differences in genome content (RNA and DNA viruses) or mode of infection (acute and persistent families of viruses). Other examples include syntenin-1 and PTPN13 able to interact with distant viral proteins such as HTLV Tax-1 (this study), but also with coronaviral E, 3A and N proteins (Caillet-Saguy et al., 2021; Jimenez-Guardeño et al., 2014). These pan-viral interactors may thus constitute ideal drug targets for the discovery of broad-spectrum antiviral inhibitors. In fact we showed

that, compared to hDLG1, syntenin-1 PDZ domains exhibit low affinities for the Tax-1 PBM peptide, as previously reported for other systems (Grembecka *et al.*, 2006a; Latysheva et al., 2006). The low affinity appears to be a general feature of the syntenin-1 PDZ-mediated binding, underlying its role in orchestrating the dynamic interaction networks, capable of rapid response to environmental changes (Manjunath et al., 2018). Consistent with the above findings, we previously highlighted the importance of syntenin-1 as a potential recruiter of proteins into extracellular vesicles (EV) (Luck *et al.*, 2020). Here, we further demonstrate that through its PDZ domains syntenin-1 recruits Tax-1 into EV exosomes (Figure 3B), providing a mechanistic explanation for the presence of the Tax-1 protein in exosomes isolated from HTLV-1-infected cell lines, HAM/TSP or ATL patient samples (Barclay et al., 2017; Jaworski et al., 2014; Otaguiri et al., 2018). A compelling hypothesis is that blocking syntenin-1/viral proteins interactions could elicit a two-pronged inhibitory activity: (i) at the viral budding step of enveloped viruses replication, where syntenin-1 could connect viral particles to the ESCRT pathway (Göttlinger *et al.*, 1991; Hanson and Cashikar, 2012; Votteler and Sundquist, 2013); and (ii) in cell-to-cell viral transmission and inflammatory immune response induction by exosomes containing syntenin-1/viral proteins complexes (Otaguiri *et al.*, 2018). Interestingly, a small molecule inhibitor of the syntenin-exosomal pathway was also shown to potentially inhibit tumor exosomal communication in breast carcinoma cells (Leblanc *et al*. 2020).

Structural basis of Tax-1-PDZ interactions

Structural insights are essential for design of small molecule inhibitors of interactions between viral proteins and cellular protein modules. X-ray structures of hDLG1 PDZ1 and PDZ2 complexes with unrelated X-S/T-X-V containing peptides show that their C-terminal carboxyl group makes hydrogen bonds with the main-chain amide protons of the conserved LGF residues (L234-G235-F236 and L329-G330-F331 in hDLG1 PDZ1 and PDZ2, respectively) (Zhang et al., 2011). Interestingly, in our NMR experiments with Tax-1 10mer, the backbone amides of G235, F236, G330, and F331 experience the largest binding shifts (Figure 2.A-B). (Note that the L234 and L329 NH resonances were not observed in this work.) Moreover, the size and direction of those effects (large downfield

shifts both in proton and nitrogen dimensions) are consistent with the formation of strong hydrogen bonds (Rance et al., 1983). These findings suggest that the C-terminal part of Tax-1 adopts the canonical binding mode displayed in the X-ray structures of hDLG1 PDZ-peptide complexes (Figure 2C-D) (Rance *et al.*, 1983; Zhang *et al.*, 2011). Comparison across different PDZ-peptide systems shows that hDLG1 residues G235, F236, G330, and F331 act as binding hot spots, which should be amenable to traditional drug discovery efforts aiming at designing potent small molecule binders. As a proof-of-concept, we demonstrated a clear correlation between PPI inhibition and impairment of Tax functions, including its transformation ability and HTLV-1 cell-to-cell transmission. The combination of our experimental strategies should allow the development of anti-Tax-1 compounds for future pre-clinical and clinical studies of drug candidates for treatment of HTLV-1-induced diseases.

Limitations of the study

In this work, we have only characterized one portion of the Tax-1 interactome, the PDZome, yet there are other host protein domains and motifs specifically interacting with HTLV-1 Tax (Table S1). Therefore, it will be important to obtain structural data for other interactions such as those involving CREB/ATF and NF-kB transcription factors, which are key drivers of the molecular mechanisms underlying HTLV-1 pathogenesis. Furthermore, the FJ9 small molecule used in this study is an indole-2-carbinol-based chemical scaffold compound that was previously identified to inhibit Frz7-DVL3 interaction (Fujii *et al.*, 2007). We envisage that other chemical structures could mimic the Tax-1 PBM binding to PDZ domain. Subsequent follow-up studies, e.g. employing computational structure-based docking methodologies (Gorgulla and Boeszoermenyi, 2020), could potentially identify more potent small-molecular inhibitors targeting the Tax-1/PDZ binding interface. Finally, although it has been shown that the Tax-1 PBM is essential to sustain T-cell proliferation in HTLV-1-infected humanized mice (Pérès and Blin, 2018), we did not examine the *in vivo* impact of inhibiting Tax-1 PBM-PDZ interaction using small molecule inhibitors.

Concluding remarks

Despite 60 years of molecular virology research, the arsenal of antiviral drugs remains dangerously small, with only ~90 molecules available today (De Clercq and Li, 2016). Those are strongly biased towards a single virus, the human immunodeficiency virus (HIV) and its key enzymes (reverse transcriptase, protease and integrase). As evidenced by the current pandemic caused by the severe acute respiratory syndrome coronavirus type 2 (SARS-CoV-2), novel antiviral drugs are needed to control viral infections effectively, in addition to vaccines and public health measures. Here we propose a predictive strategy based on prior interactome and structural information. First, bioinformatic tools could be used to systematically merge information from viral sequences, predict and validate viral products, and identify viral motifs and domains capable of interacting with host proteins. Second, the predicted interactions could be experimentally validated using the methodologies such as those developed in this study, e.g, combining interactome mapping and structural characterization. Third, identification of common host interactors across the well-known and emerging viruses might reveal promising targets for broad-spectrum antiviral drugs. Finally, potential small molecule inhibitors (repurposed or predicted) could be tested and validated in relevant biological settings. This strategy will allow integration of knowledge on distant viruses that use similar mechanisms to perturb infected cells' homeostasis and hopefully yield a comprehensive database of druggable viral-host protein pairs.

Star* Methods

Key Resource table

Resource Availability

- Lead contact
- Materials availability

Method Details

- Predicting potential Tax interactors using in-silico motif-domain and domain-domain based strategy
- Identification of Short linear motifs (SLiMs) in Tax protein sequence
- Cell culture
- Transient transfections
- Tax-1 Yeast 2 Hybrid with individual PDZ Domains
- GST-pulldown
- Gaussia princeps luciferase complementation assay (GPCA)
- Measurement of Luciferase activity
- Synthetic Peptides
- Expression and purification
- Isothermal Titration calorimetry
- Nuclear Magnetic Resonance Spectroscopy
- RNA interference
- Immunoblots
- Immunofluorescence and confocal microscopy
- qRT-PCR
- Purification of exosomes
- Tax-1 / SDCBP immunoprecipitation
- Cellular localization of Tax-1 and SDCBP
- Mutual effect of overexpression of Tax-1 and SDCBP
- Molecular Docking
- Tax-1-induced transformation inhibition test by FJ9
- Test for inhibition of cell-to-cell transmission of Tax-1 by FJ9
- Test for inhibition of the interaction of Tax-1 with SDCBP by FJ9
- Statistical analysis

Acknowledgments

We thank Dr. Fujii Naoaki (Purdue University) for providing the FJ9 compound. Computational resources have been provided by the Consortium des Équipements de Calcul Intensif (CÉCI), funded by the Fonds de la Recherche Scientifique (FRS-FNRS, Belgium) under Grant No. 2.5020.11 and by the Walloon Region. We thank the Cell Imaging and Viral Vectors core facilities of the University of Liege for their services. J.-P.B.'s lab is funded by La Ligue Nationale Contre le Cancer (Label 2019), Institut Paoli-Calmettes and Institut Universitaire de France. PZ's lab work was funded by La Ligue Nationale Contre le Cancer (Label 2018), the Fund for Scientific Research—Flanders (FWO, G0C5718N) and the internal funds of the KU Leuven (C14/20/105). This work was primarily supported by the FRS-FNRS Televie grants 30823819 to J-C.T; Fund for Research Training in Industry and Agriculture grants 24343558 and 29315509 to K.B.

Author contributions

Conceptualization, S.M., J-C.T., I.VM. and A.V.; Methodology, S.M., I.VM., A.V, C.G. and J-C.T; Investigation, S.M, I.VM, K.B., C.G., J.O.,J.B., S.S., D.S., T.N., B.L., F.L., A.B., M.H., A.V. and J-C.T.; Formal analysis, S.M., J-C.T., D.S, I.VM. and A.V Resources, JP. B., P.Z., F.D, L.W., J.VW, F.D., H.A., A.V. and JC.T. ; Writing - Original Draft, S.M., K.B., I.VM, A.V . and J-C.T.; Writing, - Review and Editing, JP. B., P.Z., F.D, L.W., J.VW, F.D., H.A., A.V. and JC.T.; Supervision, J-C.T.,A.V., H.B. and F.D.; Funding Acquisition, J-C.T.,A.V., L.W., P.Z., H.B. and F.D

Declaration of interests

The authors declare no competing interests.

Figure Legends

Figure 1. A comprehensive analysis of the Tax-1 interactome with human PDZ-containing proteins.

(A). *In silico* prediction of interactions between Tax-1 domains and motifs and human proteins domains listed in Table S1. (B) A map of Tax-1-PDZ interactome. Red indicates overlap with known PPIs from the literature. (C) Expression of the interacting PDZ-containing protein genes across 24 different T-cell lines. (D) Differential expression data in HTLV-1-infected versus non-infected T-cells (genes for which $p<0.05$ are shown). (E) Differentially expressed PDZ genes in Jurkat T-cells following induction of the Tax-1 expression (genes for which $p<0.01$ are shown). (F) PDZ genes mutated in ATL patient samples. (G) Differentially expressed PDZ genes in ATL patient samples relative to healthy carriers (genes for which $p<0.05$ are shown). (H) SAFE analysis of the Tax-1/ human PDZ proteins interactome. See also Figure S1, Tables S1

Figure 2. NMR-observed binding of the C-terminal part of Tax-1 to hDLG1 PDZ domains.

The interaction of Tax-1 10 mer peptide with ^{15}N hDLG1 (A-D) PDZ1+2 tandem or individual (E-H) PDZ1 and (I-L) PDZ2 domains. (A,E,I) Overlay of selected regions of ^{1}H,^{15}N HSQC spectra showing large binding shifts for several backbone amide resonances. The spectra of the free and Tax-1 10mer-bound ^{15}N hDLG1 PDZ domains are in black and red, respectively, with the chemical shift perturbations for the selected residues indicated by arrows. (B,F,J) Average amide binding shifts ($\Delta\delta_{avg}$) at saturating amounts of Tax-1 10mer. The horizontal lines show the average $\Delta\delta_{avg}$ and the average (avg) plus one standard deviation (stdev). Residues with large $\Delta\delta_{avg}$ are labelled. The secondary structure of the hDLG1 PDZ1 and PDZ2 domains, drawn from the PDB entries 3RL7 and 3RL8, respectively (Zhang *et al.*, 2011), is shown above the plot. (C,D,G,K) Chemical shift mapping of the Tax-1 10mer binding. The molecular surfaces of hDLG1 (C,G) PDZ1 and (D,K) PDZ2 domains are colored by the $\Delta\delta_{avg}$ values (orange: $\Delta\delta_{avg}$ > avg; red: $\Delta\delta_{avg}$ > avg + stdev). Prolines and residues with unassigned backbone amide resonances are in grey. The modeled C-terminal part of the Tax-1 peptide, bound to the canonical PDZ site, is shown in sticks. (H,L) Binding of the Tax-1 10mer observed by isothermal titration calorimetry (ITC). The top and bottom panels show, respectively, the raw data after the baseline correction and the integrated data corrected for the heat of Tax-1 10mer dilution. The solid line in the bottom panel shows the best fit to a binding model with (H) the stochiometry n = 1.03 ± 0.03, equilibrium dissociation constant K_D = 2.7 ± 0.3 μM, and the binding enthalpy ΔH = -8.0 ± 0.3 kcal/mol and (L) n = 0.99 ± 0.02, K_D = 0.9 ± 0.1 μM, and ΔH = -10.4 ± 0.2 kcal/mol

Figure 3. A crosstalk between Tax-1-PDZ interactions and membrane vesicles trafficking.
(A) Tax-1 interactome with the cytoskeleton. (B) HEK293 cells transfected with Tax in the presence of a control siRNA or SDCBP siRNA. Exosomes were purified and characterized by western blot using indicated antibodies, in comparison with whole cell lysates. (C) Confocal microscopy examination of HeLa cells expressing Tax-1 in the presence of a control siRNA or SDCBP siRNA HTLV-1 Tax (Tax-1). Bars graphs indicate relative quantification of the Alexa-fluor 488 intensities. (D) Tax-1 fused to the Gal4 DNA-binding (DB) domain, and SDCBP or SDCBP2 fused to Gal4 activating domain (AD) interact in yeast. (E) Tax-1 co-immunoprecipitates with SDCBP and SDCBP2 in transfected HEK293 cells. (F) Pulldown of indicated SDCBP (S1) and SDCBP2 (S2) domains fused to GFP using GST-Tax-1 bound to glutathione beads.

Figure 4. NMR-observed binding of the Tax-1 10mer peptide to syntenin-1 PDZ domains.
The interaction of Tax-1 10mer with ^{15}N syntenin-1 (A-B) PDZ1+2 tandem or individual (C-E) PDZ1 and (F-H) PDZ2 domains. (A,C,F) $\Delta\delta_{avg}$ in the presence of 5 molar equivalents of Tax-1 10mer. Residues with backbone amides broadened beyond the detection limit upon complex formation are indicated by red bars. The horizontal lines show the average $\Delta\delta_{avg}$ and the avg + stdev. Residues with large $\Delta\delta_{avg}$ are labelled. The secondary structure of syntenin-1 PDZ1 and PDZ2 domains, drawn from the PDB entry 1W9E(Grembecka et al., 2006b) , is shown above the plot. (B,D,G) Chemical shift mapping of the Tax-1 10mer binding. The molecular surfaces of syntenin-1 PDZ domains is colored by the $\Delta\delta_{avg}$ values (yellow: $\Delta\delta_{avg}$ > avg; orange: $\Delta\delta_{avg}$ > avg + stdev; red: broadened out upon binding). Prolines and residues with unassigned or strongly overlapping backbone amide resonances are in grey. The modeled C-terminal parts of the Tax-1 peptide, bound to the canonical PDZ sites, are shown in sticks. (E,H) NMR chemical shift titrations with the Tax-1 10mer peptide. Chemical shift perturbations of the backbone amide atoms indicated in the plots were fitted simultaneously to a binding model with the shared K_D (Equation 1). The solid lines show the best fits with (E) K_D = 2.58 ± 0.45 mM for syntenin-1 PDZ1 and (H) K_D = 1.55 ± 0.20 mM for syntenin-1 PDZ2.

Figure 5. Perturbation of the Tax-PDZ interactions and inhibition of Tax-1 functions.
(A) Structure of the small molecule FJ9. (B) Molecular docking of the small molecule FJ9 into the syntenin-1 PDZ2 domain (left), and detailed interactions between FJ9 and syntenin-1 PDZ2 residues (right). The intermolecular hydrogen bond with the backbone carbonyl atom of F211 is indicated by a dotted line. (C) Positive HEK293 cells analyzed by FACS for fluorescence intensities in the presence (300 µM) or absence (DMSO) of the FJ9 small molecule. (D) Quantification of positive BiFC cells from (C). (E) Transformation of Rat-1 fibroblast cells following Tax-1 expression and treatment with 100 µM of FJ9 in a six-well plate. (F) Quantification of Tax-1-transformed colonies from (E), considering a minimum diameter cut-off of 0.25 mm. (G) Schematic representation of the co-culture infection and inhibition assay. (H) Viability test, as measured using trypan blue, of Jurkat-LTR-Luc cells treated with DMSO, 100 µM or 300 µM of FJ9. (I) Quantification of cell-to-cell HTLV-1 transmission and inhibition

by the FJ9 small molecule. Statistical analyses were done using unpaired t-tests, where **** indicate a p value <0.0001, *** a p value <0.001, and ** a p value <0.01.

Figure S1. A comprehensive analysis of the Tax-1 interactome with human PDZ-containing proteins.

(A) PPIs between Tax-1 and human PDZ domain-containing proteins identified by yeast 2-hybrid (Y2H) and validated by GPCA, or using a pull-down assay (blue); and known PPIs from the literature (yellow). (B) Literature reported interactions between Tax-1 and human PDZ domain-containing proteins. (C) Heat maps of the Y2H assay by testing a library of 244 individualized PDZ domain-containing proteins fused to AD against DB-Tax-1. A growth score of "0", "1" or "2" indicates a null, weak or strong interaction, respectively. (D) Representative Y2H assay plate lacking tryptophan (Trp), leucine (Leu), and histidine (His) where a growth score of "0", "1" or "2" indicates a null, weak or strong interaction between DB-Tax-1 and PDZ-domain-containing proteins fused to AD, respectively. (E) Representative GST-pull-down analyses of proteins encoded by Flag-fused open reading frames (ORFs) available in the human ORFeome collection.

Figure S2. Validation of hDLG1 PDZ-Tax-1 interactions and NMR-observed binding of hDLG1 PDZ1+2 tandem to Tax 2.

(A) Purified GST-fused hDLG1 PDZ1 domains. (B) GST-pulldown assay using Tax-1 protein from HTLV-1 producing MT2 cells. (C) Overlay of selected regions of $^{1}H,^{15}N$ HSQC spectra in the absence and presence of Tax2 10mer (black and orange, respectively). The labels identify the backbone amide resonances affected by the Tax-1 10mer binding (cf. Figure 2. (D) $\Delta\delta_{avg}$ of the hDLG1 PDZ1+2 in the presence of 6 molar equivalents of Tax2 10mer. The horizontal lines show the average $\Delta\delta_{avg}$ and the avg + stdev. (E,F) Chemical shift mapping of the Tax2 10mer binding. The molecular surfaces of hDLG1 (E) PDZ1 and (F) PDZ2 domains are colored by the $\Delta\delta_{avg}$ values as in Figure 2C,D. The modeled C-terminal part of the Tax-1 peptide, bound to the canonical PDZ site, is shown in sticks as a reference. (G) Chemical shift perturbations ($\Delta\delta$) of the backbone N (left) and H (right) atoms for several hDLG1 PDZ1+2 residues indicated in the plots. The lines joining the symbols are only meant to guide the eye.

Figure S3. Control hDLG1 PDZ NMR experiments with Tax-1 PBM 4mer and N-terminal 6mer (6mer-N) peptides.

(A) Overlay of $^{1}H,^{15}N$ HSQC spectra of the free and PBM 4mer-bound ^{15}N hDLG1 PDZ1+2 tandem (in black and blue, respectively), with the chemical shift perturbations for the selected residues indicated by arrows. (B) $\Delta\delta_{avg}$ of the hDLG1 PDZ1+2 at saturating amounts of PBM 4mer. (C,D) Chemical shift mapping of the PBM 4mer binding. The molecular surfaces of hDLG1 (C) PDZ1 and (D) PDZ2 domains are colored as in Figure 2C,D. The modeled PBM peptide, bound to the canonical PDZ site, is shown in sticks. (E) The spectra of the ^{15}N hDLG1 PDZ1+2 tandem in the absence and presence of 6mer-N (black and green, respectively).(F) $\Delta\delta_{avg}$ of the hDLG1 PDZ1+2 in the presence of 6 molar equivalents of 6mer-N.The labels identify the sole residue with a significant binding shift.

Figure S4. Control NMR experiments with the C-terminally amidated Tax-1 10mer peptide (Tax-1mod).

(A) Overlay of $^{1}H,^{15}N$ HSQC spectra of ^{15}N hDLG1 PDZ1 in the absence and presence of Tax-1mod peptide (black and red, respectively). The labels identify the backbone amide resonances affected by the Tax-1 10mer binding (cf. Figure 2E). (B) $\Delta\delta_{avg}$ of hDLG1 PDZ1 at saturating amounts of Tax-1mod. (C) Chemical shift mapping of the Tax-1mod binding. The molecular surface of hDLG1 PDZ1 is colored as in Figure 2G. The modeled C-terminal part of the Tax-1 peptide, bound to the canonical PDZ site, is shown in sticks. (D) NMR chemical shift titration of ^{15}N hDLG1 PDZ1 with the Tax-1mod peptide. Open and filled symbols refer to the chemical shift perturbations ($\Delta\delta$) of the backbone H and N atoms, respectively, of F236 (squares), G240 (circles), I258 (triangles), I259 (diamonds), and L296 (stars). The curves were fitted simultaneously to a binding model with the shared K_D (Equation 1). The solid lines show the best fits with the K_D value of 951 ± 34 μM.

Figure S5. Control syntenin-1 NMR-experiments with Tax-1 PBM 4mer and 6mer-N peptides.

(A) $\Delta\delta_{avg}$ of ^{15}N syntenin-1 PDZ1+2 tandem in the presence of 6 molar equivalents of PBM 4mer. Residues with backbone amides broadened beyond the detection limit upon complex formation are indicated by red bars. (B) Chemical shift mapping of the PBM 4mer binding. The molecular surface of syntenin-1 PDZ1+2 tandem is colored as in Figure 4B. The modeled PBM peptides, bound to the canonical PDZ sites, are shown in sticks. (C) $\Delta\delta_{avg}$ of the ^{15}N syntenin-1 PDZ1+2 tandem in the presence of 7 molar equivalents of 6mer-N. Several residues with significant binding shifts are labelled.

STAR*METHODS

Key resources table

REAGENT or RESOURCE	SOURCE	IDENTIFIER
Antibodies		
Anti-Tax	Francoise Bex	Meertens et al., 2004
Anti-GAPDH	Santa Cruz	PRID: AB_2107299
Anti-GST	Santa Cruz	PRID:sc-138
Anti-Flag	Sigma-Aldrich	F3165
Chemicals		
Doxycycline hydrochloride	Fisher Scientific	Cat#10592-13-9
Protamine sulfate	MP Biomedicals	Cat#9009-65-8
Blasticidin S	Sigma-Aldrich	Cat# 15205
Hygromycin B	Sigma-Aldrich	Cat# 10843555001
$U^{13}C_6$ Glucose	Cotercnet	Cat# CC860P10
^{15}N Ammonium chloride	Cotercnet	Cat# CN80P10
Experimental Models: Cell Lines		
HeLa	ATCC	CRM-CRL-2
HEK293T	ATCC	CRL-3216
Jurkat	ATCC	CSC-C9455L
ALL-SIL	DSMZ	ACC 511
Be13	DSMZ	ACC 396
CTV-1	DSMZ	ACC 40
DND-41	DSMZ	ACC 525
DU,528		CVCL_5617
HPB-ALL	DSMZ	ACC 483
H-SB2		CVCL_1859)
Karpas 45		ECACC 06072602)
KOPT-K1		CVCL_4965
LOUCY	DSMZ	ACC 394
MOLT	DSMZ	ACC 29
P12-ICHIKAWA	DSMZ	ACC 34
PEER	DSMZ	ACC 6
PF-382	DSMZ	ACC 38
SKW-3	DSMZ	ACC 53
SUP-T11	DSMZ	ACC 605
SUP-T13		CVCL_9973

SUP-T7		CVCL_A449
C91		CVCL_0197
MT2	Sigma-Aldrich	08081401
Experimental Models: Organisms/Strains		
S.cerevisiae:Strain background: MATa Y8800	(Yu et al., 2008)	N/A
S.cerevisiae:Strain background: MATa Y8930	Yu et al., 2008)	N/A
E. coli BL21 DE3 pyLysS	Invitrogen	C602003
Recombinant DNA		
pLenti-CMVtight-Blast-DEST	Eric Campeau	Addgene#26434
pLenti CMV rtTA3	Eric Campeau	Addgene #26429
pLVX-Tet3G	Clontech-Takara	Takara Cat#631187
psPAX2	Didier Trono	Addgene # 12260
pCMV-VSVG	(Stewart, 2003)	Addgene #8454
pLenti6 Tight-Tax	This paper	N/A
pGEX6P-1 DLG1 PDZ1	Tonikian et., al 2008	Addgene# 103915
pGEX6P-1 DLG1 PDZ2	Tonikian et., al 2008	Addgene# 103916
pGEX6P-1 DLG1 PDZ3	Tonikian et., al 2008	Addgene # 103917
pGEX6P-1 DLG1 PDZ1+2	This Paper	N/A
pGEX6P-1 SDCBP1 PDZ1	This Paper	N/A
pGEX6P-1 SDCBP1 PDZ1	This Paper	N/A
pGEX6P-1 SDCBP1 PDZ1+2	This paper	N/A

Lead contact

Further information and request can be directed to Jean-Claude Twizere (jean-claude.twizere@uliege.be)

Resource Availability

Plasmids generated in this study are available upon request and approval of the Material Transfer Agreement (MTA) by the University of Liege.

METHOD DETAILS

Predicting potential Tax interactors using in-silico motif-domain and domain-domain based strategy

In order to predict potential human host targets of Tax-1, two approaches were combined similar to Zanzoni et al., 2017 (Zanzoni et al., 2017b). These were, i) Motif-domain based interaction inferences in which it was inferred that an interaction between human protein A and Tax, if Tax-1 possesses a short linear motif (SLiM), m that binds to a complementary domain d in protein A. For instance, with Tax having a PBM, if a given protein contains a PDZ domain, it is inferred as one of potential interactors of Tax. ii) Domain-domain based interaction inferences in which Tax and human host interactor protein A is predicted to interact with each other if Tax possesses an interaction domain d1 that binds with interaction domain d2 in host interactor protein A. For instance, the Zinc finger like domain in Tax-1 and it is known that zinc finger-like domains might bind to another zinc finger-like domain. Hence, a protein with zinc finger-like domain would be inferred as one of the potential interactors of Tax. All the templates for inferring motif-domain and domain-domain based interactions were retrieved from three resources a) 3did Database (Mosca et al., 2014) b) ELMdb (Dinkel et al., 2012) (Garamszegi et al., 2013) c) Garamszegi et al., 2013. In this case 535, 232 and 666 motif-domain template interactions were retrieved from 3did, ELMDb and Garamszegi et al., 2013(Garamszegi *et al.*, 2013) respectively. Finally, an exhaustive list of 1311 motif-domain based template interactions were prepared combining the three resources. Domain-domain and motif-domain interaction templates were downloaded from 3 did database, that currently stores 6290 high resolution interaction interfaces

Identification of Short linear motifs (SLiMs) in Tax protein sequence

Short linear motifs in Tax sequence were searched using SLiMSearch 2.0 tool from SLiM-Suite (Davey et al., 2011). SLiMSearch takes as input a set of motif consensus and search them against queried protein sequences, The motif consensus is represented as a regular expression and contains ordinary and special characters. Permitted ordinary characters are single-letter amino acid codes. The special characters are based on regular expression syntax as defined in the Eukaryotic Linear Motif resource(Kumar et al., 2020).To reduce the number of false positive instances of motif consensus, in our prediction method, only those motif instances which fall in disordered region of Tax sequence were retained. In order to detect motif instances, situated in disordered region of Tax sequence each motif instances was assigned a disorder score (DS_c):

$$DS_c = \sum_{p=s}^{e} DS_p / l$$

Where, DS_p is the IUPred disorder score of the residue at position p in Tax protein sequence, s is the start position of the consensus match, e is the end position of the consensus match, l is the consensus match length. Motif instances whose disorder score was greater than 0.4 were retained (Zanzoni *et al.*, 2017b; a). The rationale behind selecting motif instances located in the disordered region is that the functional SliMs are largely located in the unstructured region of protein(Edwards et al., 2012; Fuxreiter et al., 2007).

Cell culture

The HEK and HeLa cell lines were cultured in DMEM (Dulbecco's Modified Eagle's Medium) containing 10% FBS (Fetal Bovine Serum), 10% glutamine and antibiotics (Penicillin 100U / ml, Streptomycin 100 µg / ml). The lymphocyte cell lines (JURKAT, JURKAT-LTR, JPX9, CEM, CTV1, MOLT16, HUT78) were maintained in culture in RPMI medium (Roswell Park Memorial Institute medium), 10% glutamine and antibiotics (Penicillin 100U / ml, Streptomycin 100 µg / ml). The lymphocyte cell lines infected with HTLV-1 (MT2,

MT4, HUT102, C8145, C91PL) were cultured under the same conditions as the lymphocyte cell lines not infected with HTLV-1, in addition to the conditions of containment (biosafety) level L3. All cells were incubated at 37 ° C with 5% CO2.

Transient transfections

HEK cells cultured to 80% confluency in DMEM were transfected using PEI. The medium was changed before transfection, and cells were collected 24 hours after transfection. HeLa cells were transfected using Lipofectamine 2000 reagent (Invitrogen) according to the manufacturer's instructions and collected 24 hours after transfection. Cells transfected with siRNAs were cultured in DMEM culture medium at 40-50% confluence. siRNA transfection was performed with calcium phosphate using the ProFection® Mammalian Transfection System (Promega) transfection kit according to the manufacturer's instructions. The culture medium was changed 24 hours post transfection and cells were harvested 48 hours post transfection.

Tax-1 Yeast 2 Hybrid with individual PDZ Domains

Gateway cloning method was used to transfer the DNA encoding the PDZ domain into the AD yeast expression vector pACT2. All PDZ domains were transformed into the yeast haploid strain Y187 (MATa, ura3-52, his3-200, ade2-101, leu2-3, 112, gal4Δ, met-, gal80Δ, MEL1, URA3: GAL1UAS -GAL1TATA -lacZ). Similarly, the DNA fragment encoding Tax-1 was cloned into the DB yeast expression vector pGBT9, then transformed into the haploid yeast strain AH109 (MATa, trp1-901, leu2-3, 112, Ura3 -52, his3-200, gal4Δ, gal80Δ, LYS2: GAL1UAS-GAL1TATA-HIS3, GAL2UAS-GAL2TATA-ADE2, URA3: MEL1UAS-MEL1TATA-lacZ, MEL1). The interactions between each PDZ and Tax-1 were tested by conjugation of the two strains of yeast. Briefly, overnight culture of the two types of yeast (of the opposite mating type) was performed. This in a selective medium favoring diploid yeast (liquid yeast extract-Peptone-Dextrose YPAD –W Tryptophan –L Leucine) supplemented with 10% PEG for 4 h at 30 ° C. With gentle stirring. After washing with water, the yeasts were placed on a solid Tryptophan-Histidine-Leucine (-WHL) selective medium for phenotypic assay. Diploid yeasts which proliferate on the -WHL medium indicate an interaction between the two fusion proteins.

GST-pulldown

To detect the Tax-1 partners by pulldown, PDZ domains were expressed in HEK293 cells. GST-Tax-1 or GST-Tax-2 protein as negative control were expressed separately and then purified with glutathione Sepharose beads. The beads now containing the fusion proteins were then incubated with PDZ-flag containing cell lysate. The detection of Flag by immunoblot indicates an interaction between Tax-1 and the PDZ domain protein

Gaussia princeps luciferase complementation assay (GPCA)

HEK293 cells were seeded in 24-well plates, then transfected with GL1 and / or GL2 plasmids expressing the fusion proteins 24 hours later. Luciferase activity was measured on the lysates in 96-well plates. The results were normalized relative to the value of the Luciferase control Renilla. The normalized luciferase ratio was calculated as follows: NLR = co-transfection luciferase value (GL1 + GL2) / (GL1 luciferase value alone + GL2 luciferase value alone). An interaction is considered positive or validated when NLR ≥ 3.5. Cell lyses and luminescence measurements were performed in triplicate for each condition.

Measurement of Luciferase activity

Collected cells were lysed with the passive lysis buffer (Promega). For luciferase measurements, 100 µl of the lysates were used, to which the substrates Firefly and Renilla stop & glo (Promega) were added. Luciferase measurements were performed in 96-well plates using an automated DLR machine. Firefly luciferase values were normalized to R-luc values, and the calculated ratio represents luciferase activity.

Synthetic Peptides

The Tax-1 10-mer (SEKHFRETEV), Tax2 10mer (NKEEADDNGD), TAX-1 PBM 4-mer (ETEV), and Tax-1 N-ter 6-mer (SEKHFR) peptides were synthesized by Biomatik, Canada, as acetate salts of >98% purity.

Expression and purification

Plasmids harboring the PDZ domains of hDLG1 tandem PDZ1+2 and syntenin-1 (PDZ1, PDZ2 and Tandem PDZ1+PDZ2) were purchased from GeneScript,hDLG1 PDZ1,2 and 3 were obtained from addgene (Tonikian et al., 2008a) and transformed into *E. coli* BL21. A single bacterial colony was used to inoculate 5.0 mL LB and grown overnight at 37 °C, from which 1.0 mL was used as starter culture for expressing the proteins in 100 mL LB. For expression, the culture was grown at 37°C, shaking (180rpm) until $OD6_{00}$ reached 0.4-0.6 then induced by addition of IPTG to a final concentration of 1.0 mM and further grown for 4 hrs under the same conditions. The isotopically labelled U-[^{13}C,^{15}N] or U-[^{15}N] proteins were produced in *E coli* grown in the minimal medium following a published protocol (Volkov et al., 2013). GST-fused proteins were purified using glutathione sepharose 4B beads (GE HealthCare) equilibrated in 1x Phosphate Buffered Saline (PBS) buffer. Bound proteins were eluted with 50 mM Tris, pH 8, 10 mM reduced glutathione. GST tag was then cleaved off using preScission protease (Sigma) overnight at 4°C. The mixture was then loaded back to the column equilibrated in PBS, and PDZ proteins were collected from the flow-through. These were further purified using a HiPrep 16/60 Sephacryl S-100 HR size exclusion column, equilibrated in 20 mM NaPi pH 6.0, 50 mM NaCl, 2 mM DTT.

Isothermal Titration calorimetry

ITC measurements were carried out on an Microcal ITC200 calorimeter at 25 °C. All experiments were performed in 10 mM Tris pH 8.0. The PDZ proteins were loaded into the sample cell at 20 μM concentration, and 250 μM of peptides (dissolved in the same buffer) were loaded into the syringe. Titrations comprised 26 × 1.5 μL injections of peptide into the protein, with 90 s intervals. An initial injection of 0.5 μL was made and discarded during data analysis. The data were fitted to a single binding site model using the Microcal LLC ITC200 Origin software provided by the manufacturer.

Nuclear Magnetic Resonance Spectroscopy

All NMR spectra were acquired at 298 K in 20 mM sodium phosphate 50 mM NaCl pH 6.0, 2 mM DTT and 10 % D_2O for the lock on a Bruker Avance III HD 800 MHz spectrometer (equipped with a TCI cryoprobe) or a Varian Direct-Drive 600 MHz spectrometer (fitted with a PFG-Z cold probe). The data were processed in NMRPipe(Delaglio et al., 1995) and analyzed in CCPNMR(Vranken et al., 2005). The assignments of backbone resonances of the individual hDLG1 and syntenin-1 PDZ1 and PDZ2 domains were obtained from 0.7-1.1 mM U-[^{13}C,^{15}N] protein samples using a standard set of 3D BEST HNCACB, HN(CO)CACB, HNCO and HN(CA)CO experiments and aided by the published assignments(Cierpicki et al., 2005; Liu et al., 2007; Tully et al., 2012). Subsequently, the NMR assignments of the individual PDZ domains were transferred to the spectra of hDLG1 and syntenin-1 PDZ1+2 tandems and verified by standard triple-resonance experiments.

The chemical shift perturbation experiments and NMR titrations were performed by incremental addition of 10 mM stock solutions of Tax peptides to U-[^{15}N] or U-[^{13}C,^{15}N] protein samples at the initial concentration of 0.3 mM. At each increment, changes in chemical shifts of the protein resonances were monitored in 2D [^{1}H,^{15}N] HSQC spectra. The average amide chemical shift perturbations ($\Delta\delta_{avg}$) were calculated as $\Delta\delta_{avg} = (\Delta\delta_N^2/50+\Delta\delta_H^2/2)^{0.5}$, where $\Delta\delta_N$ and $\Delta\delta_H$ are the chemical shift perturbations of the amide nitrogen and proton, respectively.

The NMR titration curves were analyzed with a two-parameter nonlinear least squares fit using a one-site binding model corrected for the dilution effect(Kannt et al., 1996), Eq. 1 :

$$\Delta\delta_{binding} = 0.5\Delta\delta_0\left(A - \sqrt{A^2 - 4R}\right)$$
$$A = 1 + R + K_D\frac{[peptide]_0 + R[protein]_0}{[peptide]_0[protein]_0} \quad (1),$$

where $\Delta\delta_{binding}$ is the chemical shift perturbation at a given protein/peptide ratio; $\Delta\delta_0$ is the chemical shift perturbation at 100 % peptide bound; R is the [peptide]/[protein] ratio at a given point; $[protein]_0$ and $[peptide]_0$ are the concentrations of the starting protein sample and the peptide titrant stock solution, respectively; and K_D is the equilibrium dissociation constant.

RNA interference

The double stranded interfering RNAs (siRNAs) were purchased from Eurogentec (Liège, Belgium). The following siRNAs were used in this work:SDCBP sense (5'-GCAAGAC-CUUCCAGUAUAA-3'), SDCBP anti-sense (5'-UUAUACUGGAAGGUCUUGC-3'), and control siRNA (5′-GGCUGCUUCUAUGAUUAUGtt-3').

Immunoblots

The cells were lysed and clarified by centrifugation. After incubating the lysate for 5 min at 100 ° C in the presence of Laemmli buffer, electrophoresis was carried out on 10% SDS-PAGE, followed by immunoblotting. The following antibodies were used: anti-Flag, anti-SDCBP, anti-tax and anti-ubiquitin.

Immunofluorescence and confocal microscopy

HeLa cells were seeded on coverslips in 24-well plates for 48 hours. The cells were then washed three times at 37 °C with PBS, fixed with PBS-4% paraformaldehyde for 15 min, and then washed twice more with PBS. Cells were then permeabilized with PBS-0.5% Triton X-100 for 20 min, incubated with the PBS-FBS 20% blocking solution for 30 min, and then washed twice with PBS. After that, the cells were incubated with the corresponding primary antibody diluted in PBS-Triton X-100 0.5% for 2 hours, washed 3 times with PBS, and incubated 1 hour with the corresponding Alexa conjugated secondary antibodies (Invitrogen) diluted. 1/1000 in PBS-Triton. Finally, the cells were washed 3 times with PBS and mounted on glass coverslips with ProLonf Gold Antifade containing DAPI (life technologies). The slides were examined by confocal microscopy with Leica TCS SP2 or

Nikon A1R confocal microscope with a 60X objective. The images were taken with a resolution of 1024x1024 pixels and subsequently processed and assembled with LEICA LAS AF Lite 5 or A1R Software.

qRT-PCR

Total RNA was extracted using the GeneJET RNA purification kit (Thermo scientific). Total RNA was reverse transcribed with random primers using the RevertAid First Strand cDNA Synthesis Kit (Thermo Scientific). QPCR was performed using Roche's SYBER Green detection in the Lightcycler 480 (Roche). Quantification of mRNA was performed by relative normalization to the constitutive gene GAPDH. The relative expression levels were calculated for each gene using the ΔCt or ΔΔCt method.

Purification of exosomes

Exosomes were isolated from cell supernatants. First, 50-100 ml of the supernatants were centrifuged at 2000 xg for 20 minutes at room temperature to remove floating cells. Second, the cell-free supernatant was then centrifuged at 12,000 xg for 45 minutes and filtered (0.22 µm) to remove additional cell debris. Third, the samples were ultracentrifuged for 2 h at 100,000 g 4 ° C. The pellet containing the exosomes was washed with PBS, then centrifuge for an additional 2 hours at the same speed, and finally suspended in lysis buffer (50 mM Tris-HCl, 1% SDS, pH 7.5, supplemented with protease and phosphatase inhibitors). The lysate was stored at 4 ° C until use in Western blot.

Tax-1 / SDCBP immunoprecipitation

The interaction of Tax-1 with SDCBP was re-validated by immunoprecipitation. HEK 293T cells were transfected with Flag-Syntenin, Tax-1 and Tax-2. Fourty-eight hours after the transfection, the cells were lysed and protein expression verified by a Western blot, using specific anti-Tax-1 and anti-Flag antibodies.

Cellular localization of Tax-1 and SDCBP

HeLa cells were transfected with constructs expressing Tax-1 and control siRNA or SDCBP siRNA. Cells were fixed, permeabilized and labeled with primary anti-Tax-1 antibodies and secondary antibodies conjugated to Alexa 488 24 hours post transfection. These were then analyzed under a confocal microscope. Using Nikon A1R software, we quantified the intensities of ROI (regions of interest) which allowed to determine the cytoplasm / nucleus ratio of protein localization. Statistically significant data are indicated with * ($P < 0.05$), ** ($P < 0.01$), or *** ($P < 0.001$).

Mutual effect of overexpression of Tax-1 and SDCBP

HeLa cells were transfected with constructs expressing Tax-1 and / or Flag-SDCBP. The cells were fixed, permeabilized and labeled with anti-Tax-1 or anti-Flag antibodies and conjugated secondary antibodies Alexa 488 or Alexa 633 24 hours post transfection. These were then analyzed under a confocal microscope as described for the previous section.

Molecular Docking

The crystal structure of the complex of syntenin-1 PDZ2 and syndecan-4 peptide was retrieved from RSCB Protein Data Bank (PDB:1OBY) (Kang et al., 2003). Protein preparation wizard in the Schrodinger package was used to pre-process, minimize, and refine the protein (Sastry et al., 2013). With all water molecules removed, the missing hydrogen/side-chain atoms and appropriate charge and protonation state of the protein at pH 7.0 were assigned using the Protein Preparation wizard module in Maestro (Bell et al., 2012). Molecular dynamics simulations were performed using GPU-accelerated Amber 18 software package(Lee et al., 2018). LEAP module and antechamber were used to optimize the protein and the inhibitor, respectively. Subsequently, the restrained electrostatic potential (RESP) (Dupradeau et al., 2010) and the general amber force field (GAFF) (Wang et al., 2004) were used to generate partial atomic charges and assign the force field parameters (Hornak et al., 2006). The system was neutralized by adding four Cl^- ions. A TIP3P [28] water model of 10 Å distance was used, and the simulations were carried out using periodic boundary conditions. The Particle Mesh Ewald (PME)(Harvey

and De Fabritiis, 2009) method was employed for long-range electrostatic interactions with a 12 Å cut-off. The SHAKE algorithm (Ryckaert et al., 1977) was used to constrain all the bonds to hydrogen atoms. A 2,500-step geometric minimization was performed to remove any possible steric clashes. The topology and coordinate files were generated, and the systems were subjected to 60ns MD simulations. Finally, a post analysis of the MD trajectories was carried out by computing the binding energies, root-mean-square deviation (RMSD), and root-mean-square fluctuation (RMSF) using CPPTRAJ and PTRAJ modules (Roe and Cheatham III, 2013) implemented in the Amber 18 package.

Tax-1-induced transformation inhibition test by FJ9

To test the effect of FJ9 on the transformation of cells induced by the HTLV-1 virus, Rat-1 cells were stably transduced (rat fibroblasts) with a vector lentiviral pTax-1-IB. A pool of resistant cells (5×10^3) was seeded in DMEM / 10% FCS containing 0.33% agarose, superimposed on a layer of 0.5% agarose in a 6-well plate with 100 µM of FJ9 or DMSO. After three weeks in culture, colonies that usually form "foci" were examined under a light microscope and photos taken to quantify the effect of FJ9. The Tax-1 induced foci count was performed using ImageJ software.

Test for inhibition of cell-to-cell transmission of Tax-1 by FJ9

Virus-producing cells (MT2) were co-cultured with cells containing the gene encoding luciferase under the control of the HTLV-1 LTR5' viral promoter. The cells were grown for 24 hours in the presence or absence of 100 µM of FJ9. Luciferase activation assay was performed as described previously.

Test for inhibition of the interaction of Tax-1 with SDCBP by FJ9

To estimate the ability of FJ9 to inhibit the interaction between Tax-1 and SDCBP, the fluorescent protein YFP was used. HEK 293T cells were transfected with the C terminal fragment of YFP protein fused to SDCBP and with the N terminal fragment of YFP fused to Tax-1., The cells were then treated with 300 µM FJ9 or DMSO 24 hours later and further cultured for an additional 24 hours before flow cytometry analysis. The results represent the mean and standard deviation of three independent experiments.

Statistical analysis

The values of the graphs are presented as the mean ± standard deviation, calculated on at least three independent experiments. Significance was determined using a t test with two variables (comparison of means). The thresholds of value P (p value) are represented as follows; * = $p < 0.05$; ** = $p < 0.01$ and *** = $p < 0.001$

References

Al Sharif, S., Pinto, D.O., Mensah, G.A., Dehbandi, F., Khatkar, P., Kim, Y., Branscome, H., and Kashanchi, F. (2020). Extracellular Vesicles in HTLV-1 Communication: The Story of an Invisible Messenger. *12*. 10.3390/v12121422.

Albrecht, H., Shakhov, A.N., and Jongeneel, C.V. (1992). trans activation of the tumor necrosis factor alpha promoter by the human T-cell leukemia virus type I Tax1 protein. Journal of virology *66*, 6191-6193.

Aoyagi, T., Takahashi, M., Higuchi, M., Oie, M., Tanaka, Y., Kiyono, T., Aoyagi, Y., and Fujii, M. (2010). The PDZ domain binding motif (PBM) of human T-cell leukemia virus type 1 Tax can be substituted by heterologous PBMs from viral oncoproteins during T-cell transformation. Virus genes *40*, 193-199. 10.1007/s11262-009-0447-x.

Baietti, M.F., Zhang, Z., Mortier, E., Melchior, A., Degeest, G., Geeraerts, A., Ivarsson, Y., Depoortere, F., Coomans, C., Vermeiren, E., et al. (2012). Syndecan-syntenin-ALIX regulates the biogenesis of exosomes. Nature cell biology *14*, 677-685. 10.1038/ncb2502.

Ballard, D.W., Bohnlein, E., Lowenthal, J.W., Wano, Y., Franza, B.R., and Greene, W.C. (1988). HTLV-I tax induces cellular proteins that activate the kappa B element in the IL-2 receptor alpha gene. Science *241*, 1652-1655.

Barclay, R.A., Pleet, M.L., Akpamagbo, Y., Noor, K., Mathiesen, A., and Kashanchi, F. (2017). Isolation of Exosomes from HTLV-Infected Cells. Methods in molecular biology (Clifton, N.J.) *1582*, 57-75. 10.1007/978-1-4939-6872-5_5.

Baryshnikova, A. (2016). Systematic Functional Annotation and Visualization of Biological Networks. Cell systems *2*, 412-421. 10.1016/j.cels.2016.04.014.

Bazarbachi A. (2016). Tax fingerprint in adult T-cell leukemia. Blood. 2016 Apr 7;127(14):1737-8.

Bazarbachi, A., Suarez, F., Fields, P., and Hermine, O. (2011). How I treat adult T-cell leukemia/lymphoma. Blood *118*, 1736-1745. 10.1182/blood-2011-03-345702.

Bell, J., Cao, Y., Gunn, J., Day, T., Gallicchio, E., Zhou, Z., Levy, R., and Farid, R. (2012). PrimeX and the Schrödinger computational chemistry suite of programs.

Belotti, E., Polanowska, J., Daulat, A.M., Audebert, S., Thomé, V., Lissitzky, J.-C., Lembo, F., Blibek, K., Omi, S., and Lenfant, N. (2013a). The human PDZome: a gateway to PSD95-Disc large-zonula occludens (PDZ)-mediated functions. Molecular & Cellular Proteomics *12*, 2587-2603.

Belotti, E., Polanowska, J., Daulat, A.M., Audebert, S., Thomé, V., Lissitzky, J.C., Lembo, F., Blibek, K., Omi, S., Lenfant, N., et al. (2013b). The human PDZome: a gateway to PSD95-Disc large-zonula occludens (PDZ)-mediated functions. Molecular & cellular proteomics : MCP *12*, 2587-2603. 10.1074/mcp.O112.021022.

Béraud, C., Sun, S.-C., Ganchi, P., Ballard, D.W., and Greene, W.C. (1994). Human T-cell leukemia virus type I Tax associates with and is negatively regulated by the NF-kappa B2 p100 gene product: implications for viral latency. Molecular and Cellular Biology *14*, 1374-1382.

Boxus, M., Twizere, J.-C., Legros, S., Dewulf, J.-F., Kettmann, R., and Willems, L. (2008). The HTLV-1 tax interactome. Retrovirology *5*, 1-24.

Boxus, M., Twizere, J.-C., Legros, S., Kettmann, R., and Willems, L. (2012). Interaction of HTLV-1 Tax with minichromosome maintenance proteins accelerates the replication timing program. Blood, The Journal of the American Society of Hematology *119*, 151-160.

Caillet-Saguy, C., Durbesson, F., Rezelj, V.V., Gogl, G., and Tran, Q.D. (2021). Host PDZ-containing proteins targeted by SARS-CoV-2. 10.1111/febs.15881.

Calattini, S., Chevalier, S.A., Duprez, R., Bassot, S., Froment, A., Mahieux, R., and Gessain, A. (2005). Discovery of a new human T-cell lymphotropic virus (HTLV-3) in Central Africa. Retrovirology *2*, 1-4.

Cassonnet, P., Rolloy, C., Neveu, G., Vidalain, P.-O., Chantier, T., Pellet, J., Jones, L., Muller, M., Demeret, C., and Gaud, G. (2011). Benchmarking a luciferase complementation assay for detecting protein complexes. Nature methods *8*, 990-992.

Cho, W.-K., Jang, M.K., Huang, K., Pise-Masison, C.A., and Brady, J.N. (2010). Human T-lymphotropic virus type 1 Tax protein complexes with P-TEFb and competes for Brd4 and 7SK snRNP/HEXIM1 binding. Journal of virology *84*, 12801-12809.

Christ, L., Wenzel, E.M., Liestøl, K., Raiborg, C., Campsteijn, C., and Stenmark, H. (2016). ALIX and ESCRT-I/II function as parallel ESCRT-III recruiters in cytokinetic abscission. The Journal of cell biology *212*, 499-513. 10.1083/jcb.201507009.

Cierpicki, T., Bushweller, J.H., and Derewenda, Z.S. (2005). Probing the supramodular architecture of a multidomain protein: the structure of syntenin in solution. Structure *13*, 319-327.

Cook, L.B., and Phillips, A.A. (2021). How I treat adult T-cell leukemia/lymphoma. Blood *137*, 459-470. 10.1182/blood.2019004045.

Crenon, I., Beraud, C., Simard, P., Montagne, J., Veschambre, P., and Jalinot, P. (1993). The transcriptionally active factors mediating the effect of the HTLV-I Tax transactivator on the IL-2R alpha kappa B enhancer include the product of the c-rel proto-oncogene. Oncogene *8*, 867-875.

Davey, N.E., Haslam, N.J., Shields, D.C., and Edwards, R.J. (2011). SLiMSearch 2.0: biological context for short linear motifs in proteins. Nucleic acids research *39*, W56-W60.

De Clercq, E., and Li, G. (2016). Approved Antiviral Drugs over the Past 50 Years. Clin Microbiol Rev *29*, 695-747. 10.1128/CMR.00102-15.

Delaglio, F., Grzesiek, S., Vuister, G.W., Zhu, G., Pfeifer, J., and Bax, A. (1995). NMRPipe: a multidimensional spectral processing system based on UNIX pipes. Journal of biomolecular NMR *6*, 277-293.

Dinkel, H., Michael, S., Weatheritt, R.J., Davey, N.E., Van Roey, K., Altenberg, B., Toedt, G., Uyar, B., Seiler, M., and Budd, A. (2012). ELM—the database of eukaryotic linear motifs. Nucleic acids research *40*, D242-D251.

Dupradeau, F.-Y., Pigache, A., Zaffran, T., Savineau, C., Lelong, R., Grivel, N., Lelong, D., Rosanski, W., and Cieplak, P. (2010). The REd. Tools: Advances in RESP and ESP charge derivation and force field library building. Physical Chemistry Chemical Physics *12*, 7821-7839.

Edwards, R.J., Davey, N.E., O'Brien, K., and Shields, D.C. (2012). Interactome-wide prediction of short, disordered protein interaction motifs in humans. Molecular bioSystems *8*, 282-295. 10.1039/c1mb05212h.

Feuer, G., and Green, P.L. (2005). Comparative biology of human T-cell lymphotropic virus type 1 (HTLV-1) and HTLV-2. Oncogene *24*, 5996-6004.

Fuji, S., Fujiwara, H., Nakano, N., and Wake, A. (2016). Early application of related SCT might improve clinical outcome in adult T-cell leukemia/lymphoma. *51*, 205-211. 10.1038/bmt.2015.265.

FuJiI, M., Sassone-Corsi, P., and Verma, I.M. (1988). c-fos promoter trans-activation by the tax1 protein of human T-cell leukemia virus type I. Proceedings of the National Academy of Sciences *85*, 8526-8530.

Fujii, N., You, L., Xu, Z., Uematsu, K., Shan, J., He, B., Mikami, I., Edmondson, L.R., Neale, G., and Zheng, J. (2007). An antagonist of dishevelled protein-protein interaction suppresses β-catenin–dependent tumor cell growth. Cancer research *67*, 573-579.

Fujikawa D, Nakagawa S, Hori M, Kurokawa N, Soejima A, Nakano K, Yamochi T, Nakashima M, Kobayashi S, Tanaka Y, Iwanaga M, Utsunomiya A, Uchimaru K, Yamagishi M, Watanabe T. (2016). Polycomb-dependent epigenetic landscape in adult T-cell leukemia. Blood. 2016 Apr 7;127(14):1790-802.

Fuxreiter, M., Tompa, P., and Simon, I. (2007). Local structural disorder imparts plasticity on linear motifs. Bioinformatics (Oxford, England) *23*, 950-956. 10.1093/bioinformatics/btm035.

Garamszegi, S., Franzosa, E.A., and Xia, Y. (2013). Signatures of pleiotropy, economy and convergent evolution in a domain-resolved map of human–virus protein–protein interaction networks. PLoS Pathog *9*, e1003778.

Gessain, A., Barin, F., Vernant, J.C., Gout, O., Maurs, L., Calender, A., and de Thé, G. (1985). Antibodies to human T-lymphotropic virus type-I in patients with tropical spastic paraparesis. Lancet (London, England) *2*, 407-410. 10.1016/s0140-6736(85)92734-5.

Gorgulla, C., and Boeszoermenyi, A. (2020). An open-source drug discovery platform enables ultra-large virtual screens. *580*, 663-668. 10.1038/s41586-020-2117-z.

Göttlinger, H.G., Dorfman, T., Sodroski, J.G., and Haseltine, W.A. (1991). Effect of mutations affecting the p6 gag protein on human immunodeficiency virus particle release. Proc Natl Acad Sci U S A *88*, 3195-3199. 10.1073/pnas.88.8.3195.

Grembecka, J., Cierpicki, T., Devedjiev, Y., Derewenda, U., Kang, B.S., Bushweller, J.H., and Derewenda, Z.S. (2006a). The binding of the PDZ tandem of syntenin to target proteins. Biochemistry *45*, 3674-3683. 10.1021/bi052225y.

Grembecka, J., Cierpicki, T., Devedjiev, Y., Derewenda, U., Kang, B.S., Bushweller, J.H., and Derewenda, Z.S. (2006b). The binding of the PDZ tandem of syntenin to target proteins. Biochemistry *45*, 3674-3683.

Leblanc R, Kashyap R, Barral K, Egea-Jimenez AL, Kovalskyy D, Feracci M, Garcia M, Derviaux C, Betzi S, Ghossoub R, Platonov M, Roche P, Morelli X, Hoffer L, Zimmermann P. (2020). Pharmacological inhibition of syntenin PDZ2 domain impairs breast cancer cell activities and exosome loading with syndecan and EpCAM cargo. J Extracell Vesicles. 2020 Dec;10(2):e12039.

Haller, K., Ruckes, T., Schmitt, I., Saul, D., Derow, E., and Grassmann, R. (2000). Tax-dependent stimulation of G1 phase-specific cyclin-dependent kinases and increased expression of signal transduction genes characterize HTLV type 1-transformed T cells. AIDS research and human retroviruses *16*, 1683-1688.

Haller, K., Wu, Y., Derow, E., Schmitt, I., Jeang, K.-T., and Grassmann, R. (2002). Physical interaction of human T-cell leukemia virus type 1 Tax with cyclin-dependent kinase 4 stimulates the phosphorylation of retinoblastoma protein. Molecular and cellular biology *22*, 3327-3338.

Hanson, P.I., and Cashikar, A. (2012). Multivesicular body morphogenesis. Annual review of cell and developmental biology *28*, 337-362. 10.1146/annurev-cellbio-092910-154152.

Harhaj, E.W., and Sun, S.-C. (1999). IKKγ serves as a docking subunit of the IκB kinase (IKK) and mediates interaction of IKK with the human T-cell leukemia virus Tax protein. Journal of Biological Chemistry *274*, 22911-22914.

Harrod, R., Tang, Y., Nicot, C., Lu, H.S., Vassilev, A., Nakatani, Y., and Giam, C.-Z. (1998). An exposed KID-like domain in human T-cell lymphotropic virus type 1 Tax is responsible for the recruitment of coactivators CBP/p300. Molecular and Cellular Biology *18*, 5052-5061.

Harvey, M., and De Fabritiis, G. (2009). An implementation of the smooth particle mesh Ewald method on GPU hardware. Journal of chemical theory and computation *5*, 2371-2377.

Hasegawa, H., Sawa, H., Lewis, M.J., Orba, Y., Sheehy, N., Yamamoto, Y., Ichinohe, T., Tsunetsugu-Yokota, Y., Katano, H., and Takahashi, H. (2006). Thymus-derived leukemia-lymphoma in mice transgenic for the Tax gene of human T-lymphotropic virus type I. Nature medicine *12*, 466-472.

Higuchi, M., Tsubata, C., Kondo, R., Yoshida, S., Takahashi, M., Oie, M., Tanaka, Y., Mahieux, R., Matsuoka, M., and Fujii, M. (2007). Cooperation of NF-κB2/p100 activation and the PDZ domain binding motif signal in human T-cell leukemia virus type 1 (HTLV-1) Tax1 but not HTLV-2 Tax2 is crucial for interleukin-2-independent growth transformation of a T-cell line. Journal of virology *81*, 11900-11907.

Himes, S., Coles, L., Katsikeros, R., Lang, R., and Shannon, M. (1993). HTLV-1 tax activation of the GM-CSF and G-CSF promoters requires the interaction of NF-kB with other transcription factor families. Oncogene *8*, 3189-3197.

Hinuma, Y., Nagata, K., Hanaoka, M., Nakai, M., Matsumoto, T., Kinoshita, K.I., Shirakawa, S., and Miyoshi, I. (1981). Adult T-cell leukemia: antigen in an ATL cell line and detection of antibodies to the antigen in human sera. Proc Natl Acad Sci U S A *78*, 6476-6480. 10.1073/pnas.78.10.6476.

Hirata, A., Higuchi, M., Niinuma, A., Ohashi, M., Fukushi, M., Oie, M., Akiyama, T., Tanaka, Y., Gejyo, F., and Fujii, M. (2004a). PDZ domain-binding motif of human T-cell leukemia virus type 1 Tax oncoprotein augments the transforming activity in a rat fibroblast cell line. Virology *318*, 327-336.

Hirata, A., Higuchi, M., Niinuma, A., Ohashi, M., Fukushi, M., Oie, M., Akiyama, T., Tanaka, Y., Gejyo, F., and Fujii, M. (2004b). PDZ domain-binding motif of human T-cell leukemia virus type 1 Tax oncoprotein augments the transforming activity in a rat fibroblast cell line. Virology *318*, 327-336. 10.1016/j.virol.2003.10.006.

Hong, S., Wang, L.-C., Gao, X., Kuo, Y.-L., Liu, B., Merling, R., Kung, H.-J., Shih, H.-M., and Giam, C.-Z. (2007). Heptad repeats regulate protein phosphatase 2A recruitment to I-κB kinase γ/NF-κB essential modulator and are targeted by human T-lymphotropic virus type 1 Tax. Journal of Biological Chemistry *282*, 12119-12126.

Hornak, V., Abel, R., Okur, A., Strockbine, B., Roitberg, A., and Simmerling, C. (2006). Comparison of multiple Amber force fields and development of improved protein backbone parameters. Proteins: Structure, Function, and Bioinformatics *65*, 712-725.

Hu, C.D., Chinenov, Y., and Kerppola, T.K. (2002). Visualization of interactions among bZIP and Rel family proteins in living cells using bimolecular fluorescence complementation. Molecular cell *9*, 789-798. 10.1016/s1097-2765(02)00496-3.

Hung, A.Y., and Sheng, M. (2002). PDZ domains: structural modules for protein complex assembly. Journal of Biological Chemistry *277*, 5699-5702.

Imjeti, N.S., and Menck, K. (2017). Syntenin mediates SRC function in exosomal cell-to-cell communication. *114*, 12495-12500. 10.1073/pnas.1713433114.

Ishida, T., Jo, T., Takemoto, S., Suzushima, H., Uozumi, K., Yamamoto, K., Uike, N., Saburi, Y., Nosaka, K., Utsunomiya, A., et al. (2015). Dose-intensified chemotherapy alone or in combination with mogamulizumab in newly diagnosed aggressive adult T-cell leukaemia-lymphoma: a randomized phase II study. British journal of haematology *169*, 672-682. 10.1111/bjh.13338.

Jaworski, E., Narayanan, A., Van Duyne, R., Shabbeer-Meyering, S., Iordanskiy, S., Saifuddin, M., Das, R., Afonso, P.V., Sampey, G.C., Chung, M., et al. (2014). Human T-lymphotropic virus type 1-infected cells secrete exosomes that contain Tax protein. The Journal of biological chemistry *289*, 22284-22305. 10.1074/jbc.M114.549659.

Jiang, H., Lu, H., Schiltz, R.L., Pise-Masison, C.A., Ogryzko, V.V., Nakatani, Y., and Brady, J.N. (1999). PCAF interacts with tax and stimulates tax transactivation in a histone acetyltransferase-independent manner. Molecular and Cellular Biology *19*, 8136-8145.

Jimenez-Guardeño, J.M., Nieto-Torres, J.L., DeDiego, M.L., Regla-Nava, J.A., Fernandez-Delgado, R., Castaño-Rodriguez, C., and Enjuanes, L. (2014). The PDZ-binding motif of severe acute respiratory syndrome coronavirus envelope protein is a determinant of viral pathogenesis. PLoS Pathog *10*, e1004320. 10.1371/journal.ppat.1004320.

Jin, D.-Y., Giordano, V., Kibler, K.V., Nakano, H., and Jeang, K.-T. (1999). Role of adapter function in oncoprotein-mediated activation of NF-κB: human T-cell leukemia virus type I Tax interacts directly with IκB kinase γ. Journal of Biological Chemistry *274*, 17402-17405.

Kalyanaraman, V., Sarngadharan, M., Robert-Guroff, M., Miyoshi, I., Golde, D., and Gallo, R. (1982). A new subtype of human T-cell leukemia virus (HTLV-II) associated with a T-cell variant of hairy cell leukemia. Science *218*, 571-573.

Kamoi, K., Yamamoto, K., Misawa, A., Miyake, A., Ishida, T., Tanaka, Y., Mochizuki, M., and Watanabe, T. (2006). SUV39H1 interacts with HTLV-1 Tax and abrogates Tax transactivation of HTLV-1 LTR. Retrovirology *3*, 1-14.

Kang, B.S., Cooper, D.R., Devedjiev, Y., Derewenda, U., and Derewenda, Z.S. (2003). Molecular roots of degenerate specificity in syntenin's PDZ2 domain: reassessment of the PDZ recognition paradigm. Structure *11*, 845-853.

Kannt, A., Young, S., and Bendall, D.S. (1996). The role of acidic residues of plastocyanin in its interaction with cytochrome *f*. Biochimica et Biophysica Acta (BBA)-Bioenergetics *1277*, 115-126.

Kehn, K., de la Fuente, C., Strouss, K., Berro, R., Jiang, H., Brady, J., Mahieux, R., Pumfery, A., Bottazzi, M.E., and Kashanchi, F. (2005). The HTLV-I Tax oncoprotein targets the retinoblastoma protein for proteasomal degradation. Oncogene *24*, 525-540.

Kehn, K., Deng, L., De la Fuente, C., Strouss, K., Wu, K., Maddukuri, A., Baylor, S., Rufner, R., Pumfery, A., and Bottazzi, M.E. (2004). The role of cyclin D2 and p21/waf1 in human T-cell leukemia virus type 1 infected cells. Retrovirology *1*, 1-17.

Kim, D.K., Lee, J., Kim, S.R., Choi, D.S., Yoon, Y.J., Kim, J.H., Go, G., Nhung, D., Hong, K., Jang, S.C., et al. (2015). EVpedia: a community web portal for extracellular vesicles research. Bioinformatics (Oxford, England) *31*, 933-939. 10.1093/bioinformatics/btu741.

Kumar, M., Gouw, M., Michael, S., Sámano-Sánchez, H., Pancsa, R., Glavina, J., Diakogianni, A., Valverde, J.A., Bukirova, D., Čalyševa, J., et al. (2020). ELM-the eukaryotic linear motif resource in 2020. Nucleic Acids Res *48*, D296-d306. 10.1093/nar/gkz1030.

Kwok, R.P., Laurance, M.E., Lundblad, J.R., Goldman, P.S., Shih, H.-m., Connor, L.M., Marriott, S.J., and Goodman, R.H. (1996). Control of cAMP-regulated enhancers by the viral transactivator Tax through CREB and the co-activator CBP. Nature *380*, 642-646.

Lambourne, L., Yadav, A., Wang, Y., Desbuleux, A., Kim, D.-K., Cafarelli, T., Pons, C., Kovács, I.A., Jailkhani, N., and Schlabach, S. (2021). Binary Interactome Models of Inner-Versus Outer-Complexome Organization. bioRxiv.

Latysheva, N., Muratov, G., Rajesh, S., Padgett, M., Hotchin, N.A., Overduin, M., and Berditchevski, F. (2006). Syntenin-1 is a new component of tetraspanin-enriched microdomains: mechanisms and consequences of the interaction of syntenin-1 with CD63. Mol Cell Biol *26*, 7707-7718. 10.1128/mcb.00849-06.

Lee, S.S., Weiss, R.S., and Javier, R.T. (1997). Binding of human virus oncoproteins to hDlg/SAP97, a mammalian homolog of the Drosophila discs large tumor suppressor protein. Proc Natl Acad Sci U S A *94*, 6670-6675. 10.1073/pnas.94.13.6670.

Lee, T.-S., Cerutti, D.S., Mermelstein, D., Lin, C., LeGrand, S., Giese, T.J., Roitberg, A., Case, D.A., Walker, R.C., and York, D.M. (2018). GPU-accelerated molecular dynamics and free energy methods in Amber18: performance enhancements and new features. Journal of chemical information and modeling *58*, 2043-2050.

Legros, S., Boxus, M., Dewulf, J.F., Dequiedt, F., Kettmann, R., and Twizere, J.-C. (2009). Protein-protein interactions and gene expression regulation in HTLV-1 infected cells. Frontiers in bioscience: a journal and virtual library *14*, 4138-4148.

Legros, S., Boxus, M., Gatot, J.-S., Van Lint, C., Kruys, V., Kettmann, R., Twizere, J.-C., and Dequiedt, F. (2011). The HTLV-1 Tax protein inhibits formation of stress granules by interacting with histone deacetylase 6. Oncogene *30*, 4050-4062.

Leung, K., and Nabel, G.J. (1988). HTLV-1 transactivator induces interleukin-2 receptor expression through an NF-κB-like factor. Nature *333*, 776-778.

Liu, Y., Henry, G.D., Hegde, R.S., and Baleja, J.D. (2007). Solution structure of the hDlg/SAP97 PDZ2 domain and its mechanism of interaction with HPV-18 papillomavirus E6 protein. Biochemistry *46*, 10864-10874.

Liu, Y., Wang, Y., Yamakuchi, M., Masuda, S., Tokioka, T., Yamaoka, S., Maruyama, I., and Kitajima, I. (2001). Phosphoinositide-3 kinase-PKB/Akt pathway activation is involved in fibroblast Rat-1 transformation by human T-cell leukemia virus type I tax. Oncogene *20*, 2514-2526.
Luck, K., Kim, D.K., and Lambourne, L. (2020). A reference map of the human binary protein interactome. *580*, 402-408. 10.1038/s41586-020-2188-x.

Manjunath, G.P., Ramanujam, P.L., and Galande, S. (2018). Structure function relations in PDZ-domain-containing proteins: Implications for protein networks in cellular signalling. Journal of biosciences *43*, 155-171.

Martinez, M.P., Al-Saleem, J., and Green, P.L. (2019). Comparative virology of HTLV-1 and HTLV-2. Retrovirology *16*, 1-12.

Maruyama, M., Shibuya, H., Harada, H., Hatakeyama, M., Seiki, M., Fujita, T., Inoue, J.-i., Yoshida, M., and Taniguchi, T. (1987). Evidence for aberrant activation of the interleukin-2 autocrine loop by HTLV-1-encoded p40x and T3/Ti complex triggering. Cell *48*, 343-350.

Marziali, F., Bugnon Valdano, M., Brunet Avalos, C., Moriena, L., Cavatorta, A.L., and Gardiol, D. (2017). Interference of HTLV-1 Tax Protein with Cell Polarity Regulators: Defining the Subcellular Localization of the Tax-DLG1 Interaction. Viruses *9*. 10.3390/v9120355.

Mosca, R., Ceol, A., Stein, A., Olivella, R., and Aloy, P. (2014). 3did: a catalog of domain-based interactions of known three-dimensional structure. Nucleic acids research *42*, D374-D379.

Nasr, R., Marçais, A., Hermine, O., and Bazarbachi, A. (2017). Overview of Targeted Therapies for Adult T-Cell Leukemia/Lymphoma. Methods in molecular biology (Clifton, N.J.) *1582*, 197-216. 10.1007/978-1-4939-6872-5_15.

Nejmeddine, M., Barnard, A.L., Tanaka, Y., Taylor, G.P., and Bangham, C.R. (2005). Human T-lymphotropic virus, type 1, tax protein triggers microtubule reorientation in the virological synapse. Journal of Biological Chemistry *280*, 29653-29660.

Neuveut, C., and Jeang, K.-T. (2000). HTLV-I Tax and cell cycle progression. Progress in cell cycle research, 157-162.

Neuveut, C., and Jeang, K.-T. (2002). Cell cycle dysregulation by HTLV-I: role of the tax oncoprotein. Front Biosci *7*, d157-d163.

Ohsugi, T., Kumasaka, T., Okada, S., and Urano, T. (2007). The Tax protein of HTLV-1 promotes oncogenesis in not only immature T cells but also mature T cells. Nature medicine *13*, 527-528.

Otaguiri, K.K., Dos Santos, D.F., Slavov, S.N., Depieri, L.V., Palma, P.V.B., Meirelles, F.V., Covas, D.T., da Silveira, J.C., and Kashima, S. (2018). TAX-mRNA-Carrying Exosomes from Human T Cell Lymphotropic Virus Type 1-Infected Cells Can Induce Interferon-Gamma Production In Vitro. AIDS Res Hum Retroviruses *34*, 1075-1082. 10.1089/aid.2018.0115.

Pasquier, A., Alais, S., Roux, L., Thoulouze, M.I., Alvarez, K., Journo, C., Dutartre, H., and Mahieux, R. (2018). How to Control HTLV-1-Associated Diseases: Preventing de Novo Cellular Infection Using Antiviral Therapy. Front Microbiol *9*, 278. 10.3389/fmicb.2018.00278.

Peloponese Jr, J.-M., and Jeang, K.-T. (2006). Role for Akt/protein kinase B and activator protein-1 in cellular proliferation induced by the human T-cell leukemia virus type 1 tax oncoprotein. Journal of Biological Chemistry *281*, 8927-8938.

Pérès, E., and Blin, J. (2018). PDZ domain-binding motif of Tax sustains T-cell proliferation in HTLV-1-infected humanized mice. *14*, e1006933. 10.1371/journal.ppat.1006933.

Pinto, D.O., DeMarino, C., Pleet, M.L., Cowen, M., Branscome, H., Al Sharif, S., Jones, J., Dutartre, H., Lepene, B., Liotta, L.A., et al. (2019). HTLV-1 Extracellular Vesicles Promote Cell-to-Cell Contact. Front Microbiol *10*, 2147. 10.3389/fmicb.2019.02147.

Poiesz, B.J., Ruscetti, F.W., Reitz, M.S., Kalyanaraman, V., and Gallo, R.C. (1981). Isolation of a new type C retrovirus (HTLV) in primary uncultured cells of a patient with Sezary T-cell leukaemia. Nature *294*, 268-271.

Rance, M., Sørensen, O., Bodenhausen, G., Wagner, G., Ernst, R., and Wüthrich, K. (1983). Improved spectral resolution in COSY 1H NMR spectra of proteins via double quantum filtering. Biochemical and biophysical research communications *117*, 479-485.

Roe, D.R., and Cheatham III, T.E. (2013). PTRAJ and CPPTRAJ: software for processing and analysis of molecular dynamics trajectory data. Journal of chemical theory and computation *9*, 3084-3095.

Rozenblatt-Rosen, O., Deo, R.C., Padi, M., Adelmant, G., Calderwood, M.A., Rolland, T., Grace, M., Dricot, A., Askenazi, M., Tavares, M., et al. (2012). Interpreting cancer genomes using systematic host network perturbations by tumour virus proteins. Nature *487*, 491-495. 10.1038/nature11288.

Ryckaert, J.-P., Ciccotti, G., and Berendsen, H.J. (1977). Numerical integration of the cartesian equations of motion of a system with constraints: molecular dynamics of n-alkanes. Journal of computational physics *23*, 327-341.

Sastry, G.M., Adzhigirey, M., Day, T., Annabhimoju, R., and Sherman, W. (2013). Protein and ligand preparation: parameters, protocols, and influence on virtual screening enrichments. Journal of computer-aided molecular design *27*, 221-234.

Sheng, M., and Sala, C. (2001). PDZ domains and the organization of supramolecular complexes. Annual review of neuroscience *24*, 1-29. 10.1146/annurev.neuro.24.1.1.

Simonis, N., Rual, J.-F., Lemmens, I., Boxus, M., Hirozane-Kishikawa, T., Gatot, J.-S., Dricot, A., Hao, T., Vertommen, D., and Legros, S. (2012a). Host-pathogen interactome mapping for HTLV-1 and-2 retroviruses. Retrovirology *9*, 1-20.

Simonis, N., Rual, J.F., Lemmens, I., Boxus, M., Hirozane-Kishikawa, T., Gatot, J.S., Dricot, A., Hao, T., Vertommen, D., Legros, S., et al. (2012b). Host-pathogen interactome mapping for HTLV-1 and -2 retroviruses. Retrovirology *9*, 26. 10.1186/1742-4690-9-26.

Suzuki, T., Ohsugi, Y., Uchida-Toita, M., Akiyama, T., and Yoshida, M. (1999). Tax oncoprotein of HTLV-1 binds to the human homologue of Drosophila discs large tumor suppressor protein, hDLG, and perturbs its function in cell growth control. Oncogene *18*, 5967-5972. 10.1038/sj.onc.1203008.

Tang, K.W., Alaei-Mahabadi, B., Samuelsson, T., Lindh, M., and Larsson, E. (2013). The landscape of viral expression and host gene fusion and adaptation in human cancer. Nature communications *4*, 2513. 10.1038/ncomms3513.

Taylor, J.M., and Nicot, C. (2008). HTLV-1 and apoptosis: role in cellular transformation and recent advances in therapeutic approaches. Apoptosis *13*, 733-747.

Thomas, M., and Banks, L. (2018). Upsetting the Balance: When Viruses Manipulate Cell Polarity Control. J Mol Biol *430*, 3481-3503. 10.1016/j.jmb.2018.04.016.

Tonikian, R., Zhang, Y., Sazinsky, S.L., Currell, B., Yeh, J.-H., Reva, B., Held, H.A., Appleton, B.A., Evangelista, M., and Wu, Y. (2008a). A specificity map for the PDZ domain family. PLoS biology *6*, e239.

Tonikian, R., Zhang, Y., Sazinsky, S.L., Currell, B., Yeh, J.H., Reva, B., Held, H.A., Appleton, B.A., Evangelista, M., Wu, Y., et al. (2008b). A specificity map for the PDZ domain family. PLoS biology *6*, e239. 10.1371/journal.pbio.0060239.

Tsubata, C., Higuchi, M., Takahashi, M., Oie, M., Tanaka, Y., Gejyo, F., and Fujii, M. (2005). PDZ domain-binding motif of human T-cell leukemia virus type 1 Tax oncoprotein is essential for the interleukin 2 independent growth induction of a T-cell line. Retrovirology *2*, 1-7.

Tully, M.D., Grossmann, J.G.n., Phelan, M., Pandelaneni, S., Leyland, M., and Lian, L.-Y. (2012). Conformational characterization of synapse-associated protein 97 by nuclear magnetic resonance and small-angle X-ray scattering shows compact and elongated forms. Biochemistry *51*, 899-908.

Twizere, J.-C., Kruys, V., Lefèbvre, L., Vanderplasschen, A., Collete, D., Debacq, C., Lai, W.S., Jauniaux, J.-C., Bernstein, L.R., and Semmes, O.J. (2003). Interaction of retroviral Tax oncoproteins with tristetraprolin and regulation of tumor necrosis factor-α expression. Journal of the National Cancer Institute *95*, 1846-1859.

Twizere, J.-C., Springael, J.-Y., Boxus, M., Burny, A., Dequiedt, F., Dewulf, J.-F., Duchateau, J., Portetelle, D., Urbain, P., and Lint, C.V. (2007). Human T-cell leukemia virus type-1 Tax oncoprotein regulates G-protein signaling. Blood *109*, 1051-1060.

Utsunomiya, A., Choi, I., Chihara, D., and Seto, M. (2015). Recent advances in the treatment of adult T-cell leukemia-lymphomas. Cancer science *106*, 344-351. 10.1111/cas.12617.

Vandermeulen, C., O'Grady, T., Galvan, B., Cherkaoui, M., Desbuleux, A., Coppin, G., Olivet, J., Ameur, L.B., Kataoka, K., and Ogawa, S. (2021). The viral oncoproteins Tax and HBZ reprogram the cellular mRNA splicing landscape. bioRxiv.

Volkov, A.N., Wohlkonig, A., Soror, S.H., and van Nuland, N.A. (2013). Expression, purification, characterization, and solution nuclear magnetic resonance study of highly deuterated yeast cytochrome c peroxidase with enhanced solubility. Biochemistry *52*, 2165-2175.

Votteler, J., and Sundquist, W.I. (2013). Virus budding and the ESCRT pathway. Cell host & microbe *14*, 232-241. 10.1016/j.chom.2013.08.012.

Vranken, W.F., Boucher, W., Stevens, T.J., Fogh, R.H., Pajon, A., Llinas, M., Ulrich, E.L., Markley, J.L., Ionides, J., and Laue, E.D. (2005). The CCPN data model for NMR spectroscopy: development of a software pipeline. Proteins: Structure, Function, and Bioinformatics *59*, 687-696.

Wang, J., Wolf, R.M., Caldwell, J.W., Kollman, P.A., and Case, D.A. (2004). Development and testing of a general amber force field. Journal of computational chemistry *25*, 1157-1174.
Watanabe, T., Kawakami, E., Shoemaker, J.E., Lopes, T.J., Matsuoka, Y., Tomita, Y., Kozuka-Hata, H., Gorai, T., Kuwahara, T., Takeda, E., et al. (2014). Influenza virus-host interactome screen as a platform for antiviral drug development. Cell host & microbe *16*, 795-805. 10.1016/j.chom.2014.11.002.

Winter, H.Y., and Marriott, S.J. (2007). Human T-cell leukemia virus type 1 Tax enhances serum response factor DNA binding and alters site selection. Journal of virology *81*, 6089-6098.
Wolfe, N.D., Heneine, W., Carr, J.K., Garcia, A.D., Shanmugam, V., Tamoufe, U., Torimiro, J.N., Prosser, A.T., LeBreton, M., and Mpoudi-Ngole, E. (2005). Emergence of unique primate

T-lymphotropic viruses among central African bushmeat hunters. Proceedings of the National Academy of Sciences *102*, 7994-7999.

Wu, K., Bottazzi, M.E., De La Fuente, C., Deng, L., Gitlin, S.D., Maddukuri, A., Dadgar, S., Li, H., Vertes, A., and Pumfery, A. (2004). Protein profile of tax-associated complexes. Journal of Biological Chemistry *279*, 495-508.

Wu, X., and Sun, S.C. (2007). Retroviral oncoprotein Tax deregulates NF-κB by activating Tak1 and mediating the physical association of Tak1–IKK. EMBO reports *8*, 510-515.

Xiao, G., Cvijic, M.E., Fong, A., Harhaj, E.W., Uhlik, M.T., Waterfield, M., and Sun, S.C. (2001). Retroviral oncoprotein Tax induces processing of NF-κB2/p100 in T cells: evidence for the involvement of IKKα. The EMBO journal *20*, 6805-6815.

Xie, L., Yamamoto, B., Haoudi, A., Semmes, O.J., and Green, P.L. (2006). PDZ binding motif of HTLV-1 Tax promotes virus-mediated T-cell proliferation in vitro and persistence in vivo. Blood *107*, 1980-1988.

Yan, P., Fu, J., Qu, Z., Li, S., Tanaka, T., Grusby, M.J., and Xiao, G. (2009). PDLIM2 suppresses human T-cell leukemia virus type I Tax-mediated tumorigenesis by targeting Tax into the nuclear matrix for proteasomal degradation. Blood, The Journal of the American Society of Hematology *113*, 4370-4380.

Yin, M.-J., Christerson, L.B., Yamamoto, Y., Kwak, Y.-T., Xu, S., Mercurio, F., Barbosa, M., Cobb, M.H., and Gaynor, R.B. (1998). HTLV-I Tax protein binds to MEKK1 to stimulate IκB kinase activity and NF-κB activation. Cell *93*, 875-884.

Ying, Y., and Tao, Q. (2009). Epigenetic disruption of the WNT/ß-catenin signaling pathway in human cancers. Epigenetics *4*, 307-312.

Yoshida, M. (2001). Multiple viral strategies of HTLV-1 for dysregulation of cell growth control. Annual review of immunology *19*, 475-496.

Yoshie, O. (2005). Expression of CCR4 in adult T-cell leukemia. Leukemia & lymphoma *46*, 185-190. 10.1080/10428190400007607.

Yoshie, O., Fujisawa, R., Nakayama, T., Harasawa, H., Tago, H., Izawa, D., Hieshima, K., Tatsumi, Y., Matsushima, K., Hasegawa, H., et al. (2002). Frequent expression of CCR4 in adult T-cell leukemia and human T-cell leukemia virus type 1-transformed T cells. Blood *99*, 1505-1511. 10.1182/blood.v99.5.1505.

Zanzoni, A., Spinelli, L., Braham, S., and Brun, C. (2017a). Perturbed human sub-networks by Fusobacterium nucleatum candidate virulence proteins. Microbiome *5*, 1-17.
Zanzoni, A., Spinelli, L., Braham, S., and Brun, C. (2017b). Perturbed human sub-networks by Fusobacterium nucleatum candidate virulence proteins. Microbiome *5*, 89. 10.1186/s40168-017-0307-1.

Zhang, Z., Li, H., Chen, L., Lu, X., Zhang, J., Xu, P., Lin, K., and Wu, G. (2011). Molecular basis for the recognition of adenomatous polyposis coli by the Discs Large 1 protein. PloS one *6*, e23507.

Figure 1. A comprehensive analysis of the Tax-1 interactome with human PDZ-containing proteins.

(A). *In silico* prediction of interactions between Tax-1 domains and motifs and human proteins domains listed in Table S1. (B) A map of Tax-1-PDZ interactome. Red indicates overlap with known PPIs from the literature. (C) Expression of the interacting PDZ-containing protein genes across 24 different T-cell lines. (D) Differential expression data in HTLV-1-infected versus non-infected T-cells (genes for which $p<0.05$ are shown). (E) Differentially expressed PDZ genes in Jurkat T-cells following induction of the Tax-1 expression (genes for which $p<0.01$ are shown). (F) PDZ genes mutated in ATL patient samples. (G) Differentially expressed PDZ genes in ATL patient samples relative to healthy carriers (genes for which $p<0.05$ are shown). (H) SAFE analysis of the Tax-1/ human PDZ proteins interactome. See also Figure S1, Tables S1

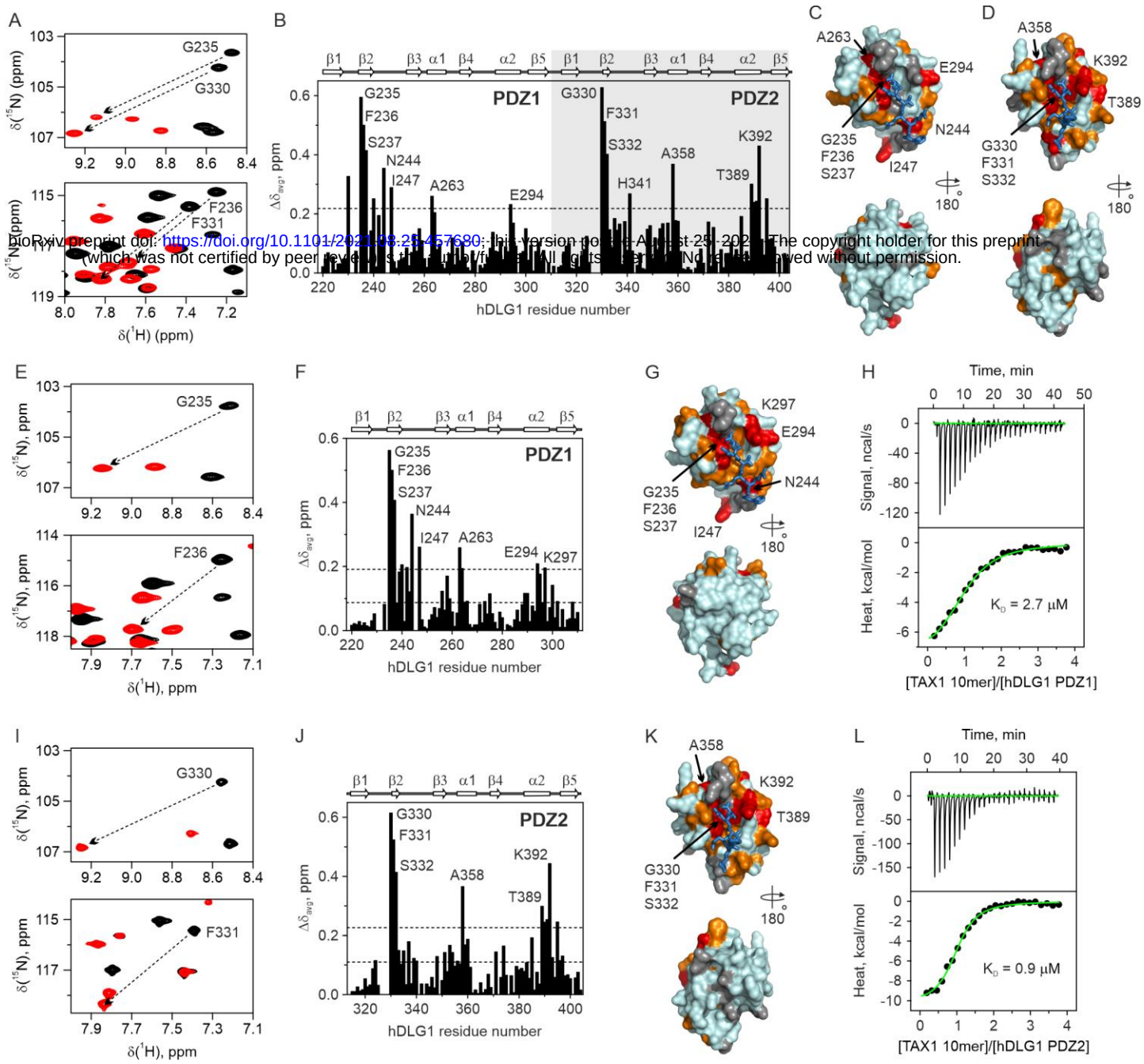

Figure 2. NMR-observed binding of the C-terminal part of Tax-1 to hDLG1 PDZ domains.
The interaction of Tax-1 10 mer peptide with ^{15}N hDLG1 (A-D) PDZ1+2 tandem or individual (E-H) PDZ1 and (I-L) PDZ2 domains. (A,E,I) Overlay of selected regions of ^{1}H,^{15}N HSQC spectra showing large binding shifts for several backbone amide resonances. The spectra of the free and Tax-1 10mer-bound ^{15}N hDLG1 PDZ domains are in black and red, respectively, with the chemical shift perturbations for the selected residues indicated by arrows. (B,F,J) Average amide binding shifts ($\Delta\delta_{avg}$) at saturating amounts of Tax-1 10mer. The horizontal lines show the average $\Delta\delta_{avg}$ and the average (avg) plus one standard deviation (stdev). Residues with large $\Delta\delta_{avg}$ are labelled. The secondary structure of the hDLG1 PDZ1 and PDZ2 domains, drawn from the PDB entries 3RL7 and 3RL8, respectively (Zhang *et al.*, 2011), is shown above the plot. (C,D,G,K) Chemical shift mapping of the Tax-1 10mer binding. The molecular surfaces of hDLG1 (C,G) PDZ1 and (D,K) PDZ2 domains are colored by the $\Delta\delta_{avg}$ values (orange: $\Delta\delta_{avg}$ > avg; red: $\Delta\delta_{avg}$ > avg + stdev). Prolines and residues with unassigned backbone amide resonances are in grey. The modeled C-terminal part of the Tax-1 peptide, bound to the canonical PDZ site, is shown in sticks. (H,L) Binding of the Tax-1 10mer observed by isothermal titration calorimetry (ITC). The top and bottom panels show, respectively, the raw data after the baseline correction and the integrated data corrected for the heat of Tax-1 10mer dilution. The solid line in the bottom panel shows the best fit to a binding model with (H) the stochiometry n = 1.03 ± 0.03, equilibrium dissociation constant K_D = 2.7 ± 0.3 μM, and the binding enthalpy ΔH = -8.0 ± 0.3 kcal/mol and (L) n = 0.99 ± 0.02, K_D = 0.9 ± 0.1 μM, and ΔH = -10.4 ± 0.2 kcal/mol

Figure 3. A crosstalk between Tax-1-PDZ interactions and membrane vesicles trafficking.

(A) Tax-1 interactome with the cytoskeleton. (B) HEK293 cells transfected with Tax in the presence of a control siRNA or SDCBP siRNA. Exosomes were purified and characterized by western blot using indicated antibodies, in comparison with whole cell lysates. (C) Confocal microscopy examination of HeLa cells expressing Tax-1 in the presence of a control siRNA or SDCBP siRNA HTLV-1 Tax (Tax-1). Bars graphs indicate relative quantification of the Alexa-fluor 488 intensities. (D) Tax-1 fused to the Gal4 DNA-binding (DB) domain, and SDCBP or SDCBP2 fused to Gal4 activating domain (AD) interact in yeast. (E) Tax-1 co-immunoprecipitates with SDCBP and SDCBP2 in transfected HEK293 cells. (F) Pulldown of indicated SDCBP (S1) and SDCBP2 (S2) domains fused to GFP using GST-Tax-1 bound to glutathione beads.

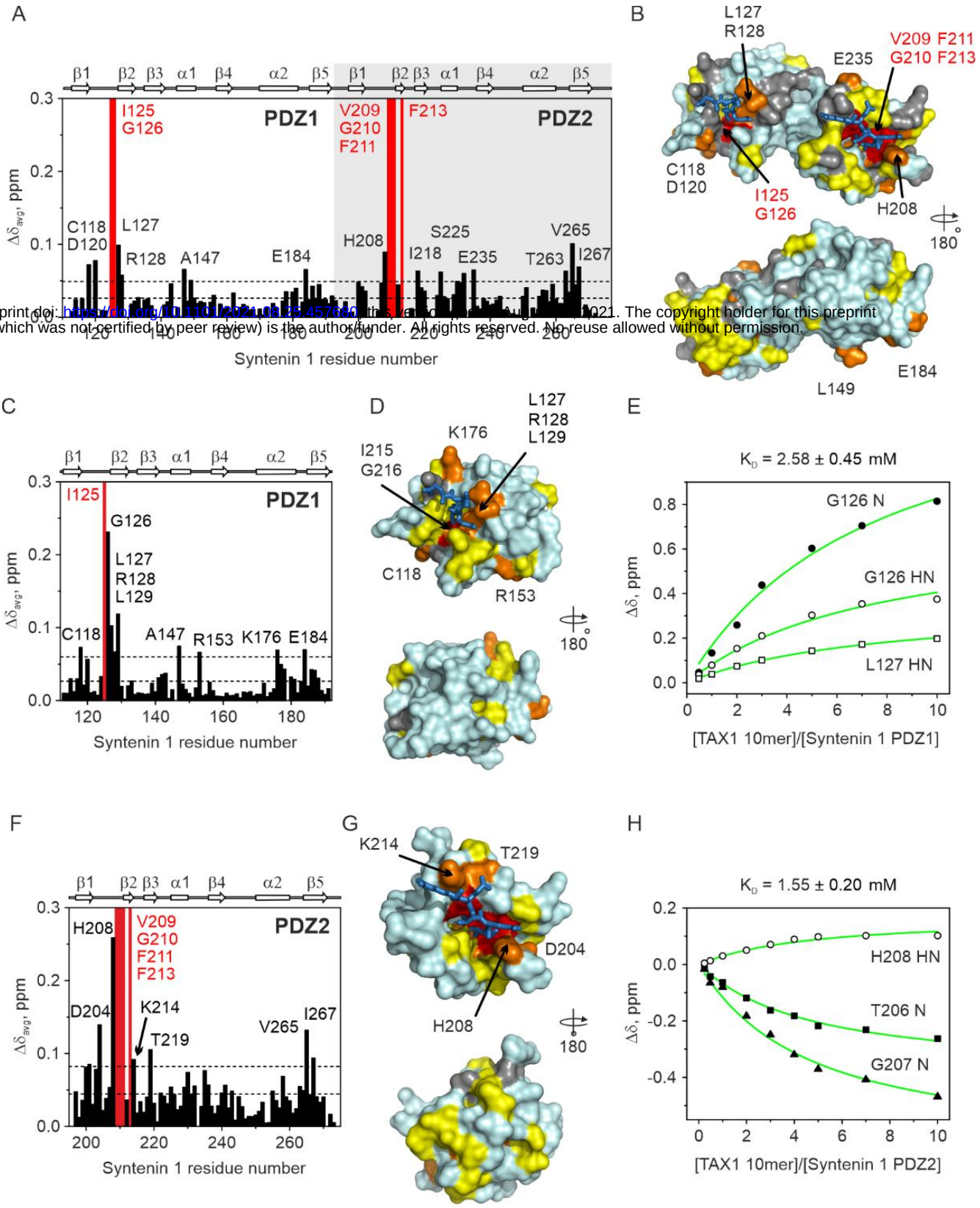

Figure 4. NMR-observed binding of the Tax-1 10mer peptide to syntenin-1 PDZ domains.
The interaction of Tax-1 10mer with ^{15}N syntenin-1 (A-B) PDZ1+2 tandem or individual (C-E) PDZ1 and (F-H) PDZ2 domains. (A,C,F) $\Delta\delta_{avg}$ in the presence of 5 molar equivalents of Tax-1 10mer. Residues with backbone amides broadened beyond the detection limit upon complex formation are indicated by red bars. The horizontal lines show the average $\Delta\delta_{avg}$ and the avg + stdev. Residues with large $\Delta\delta_{avg}$ are labelled. The secondary structure of syntenin-1 PDZ1 and PDZ2 domains, drawn from the PDB entry 1W9E(Grembecka et al., 2006b) , is shown above the plot. (B,D,G) Chemical shift mapping of the Tax-1 10mer binding. The molecular surfaces of syntenin-1 PDZ domains is colored by the $\Delta\delta_{avg}$ values (yellow: $\Delta\delta_{avg}$ > avg; orange: $\Delta\delta_{avg}$ > avg + stdev; red: broadened out upon binding). Prolines and residues with unassigned or strongly overlapping backbone amide resonances are in grey. The modeled C-terminal parts of the Tax-1 peptide, bound to the canonical PDZ sites, are shown in sticks. (E,H) NMR chemical shift titrations with the Tax-1 10mer peptide. Chemical shift perturbations of the backbone amide atoms indicated in the plots were fitted simultaneously to a binding model with the shared K_D (Equation 1). The solid lines show the best fits with (E) K_D = 2.58 ± 0.45 mM for syntenin-1 PDZ1 and (H) K_D = 1.55 ± 0.20 mM for syntenin-1 PDZ2.

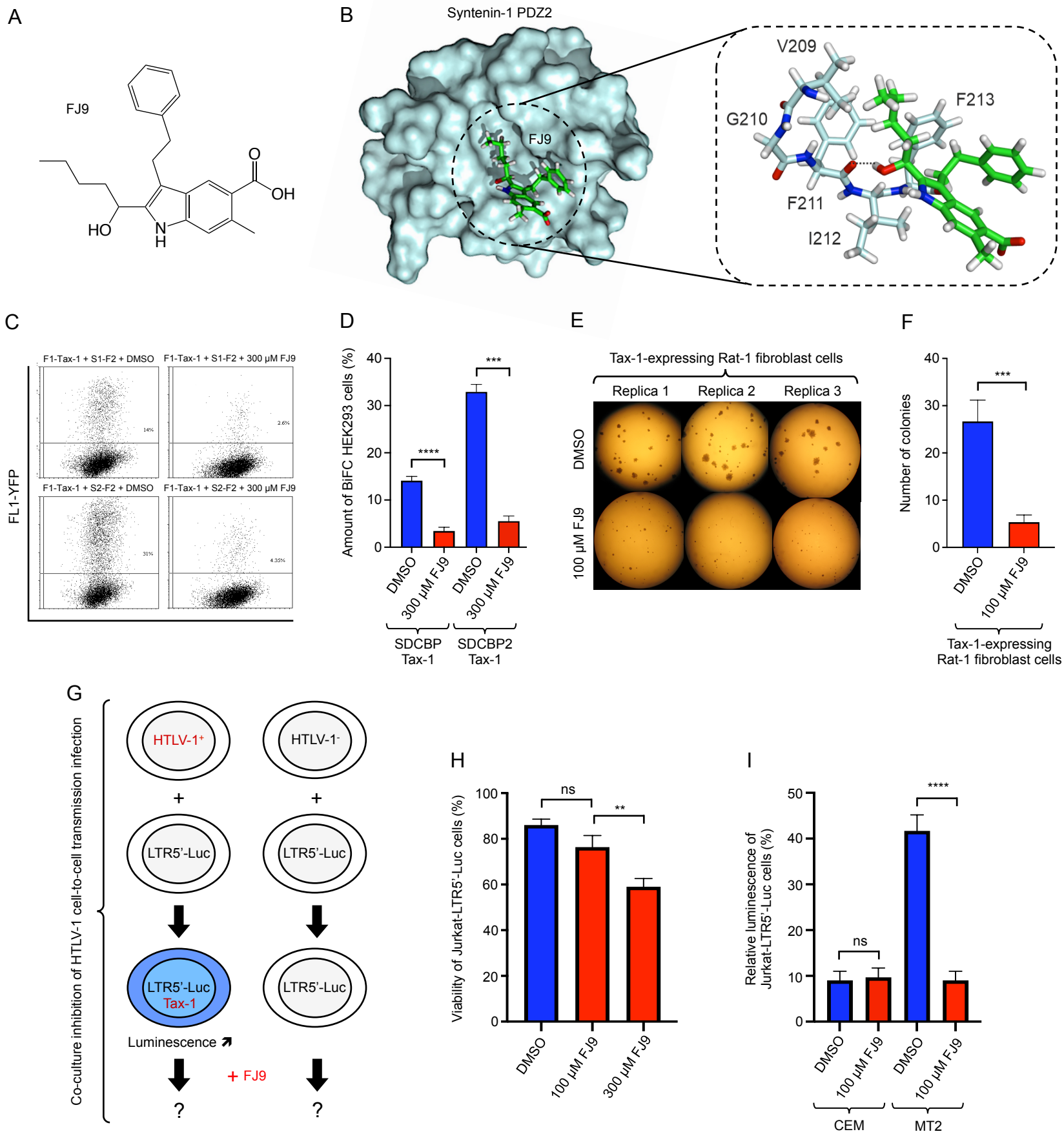

Figure 5. Perturbation of the Tax-PDZ interactions and inhibition of Tax-1 functions.

(A) Structure of the small molecule FJ9. (B) Molecular docking of the small molecule FJ9 into the syntenin-1 PDZ2 domain (left), and detailed interactions between FJ9 and syntenin-1 PDZ2 residues (right). The intermolecular hydrogen bond with the backbone carbonyl atom of F211 is indicated by a dotted line. (C) Positive HEK293 cells analyzed by FACS for fluorescence intensities in the presence (300 µM) or absence (DMSO) of the FJ9 small molecule. (D) Quantification of positive BiFC cells from (C). (E) Transformation of Rat-1 fibroblast cells following Tax-1 expression and treatment with 100 µM of FJ9 in a six-well plate. (F) Quantification of Tax-1-transformed colonies from (E), considering a minimum diameter cut-off of 0.25 mm. (G) Schematic representation of the co-culture infection and inhibition assay. (H) Viability test, as measured using trypan blue, of Jurkat-LTR-Luc cells treated with DMSO, 100 µM or 300 µM of FJ9. (I) Quantification of cell-to-cell HTLV-1 transmission and inhibition by the FJ9 small molecule. Statistical analyses were done using unpaired t-tests, where **** indicate a p value <0.0001, *** a p value <0.001, and ** a p value <0.01.

A

B

Tax-1 protein partner (gene symbol)	Gene ID	UniProt ID	PubMed ID	HTLV-1 biology
DLG1	1739	Q12959	9192623	Cell cycle acceleration
DLG4	1742	P78352	9482110	
ERBB2IP	55914	Q96RT1	17100642	
IL16	3603	Q14005	12620798	Cell cycle acceleration
LIN7A	8825	O14910	9482110	
LNX2	222484	Q8N448	22458338	
MAGI1	9223	Q96QZ7	23279616	IL-2-independent growth
MAGI3	260425	Q5TCQ9	15003862	
PARD6A	50855	Q9NPB6	9482110	
PDLIM2	64236	Q96JY6	19131544	Tax-mediated tumorigenesis
SCRIB	23513	Q14160	17855372	Immune response suppression
SNTB1	6641	Q13884	9482110	
SNTB2	6645	Q13425	9482110	
TAX1BP3	30851	O14907	9482110	

C

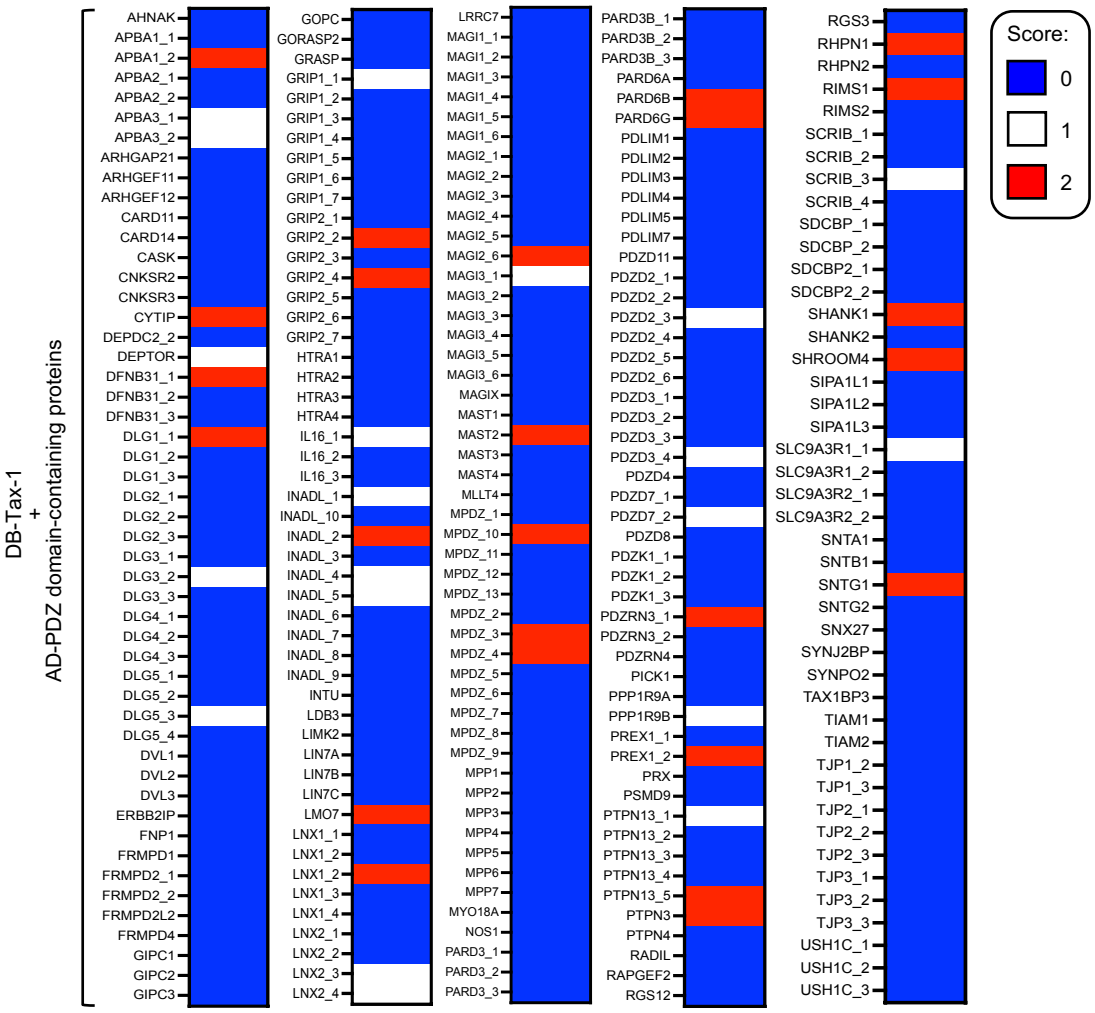

D

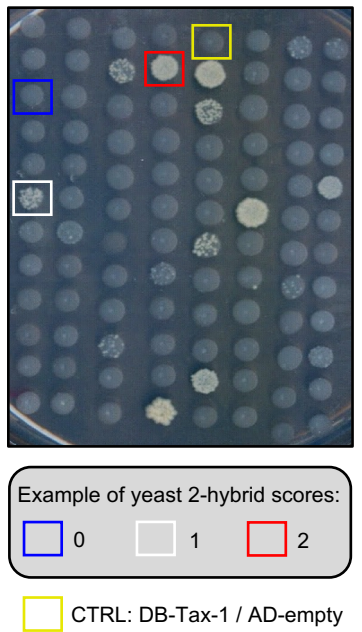

E

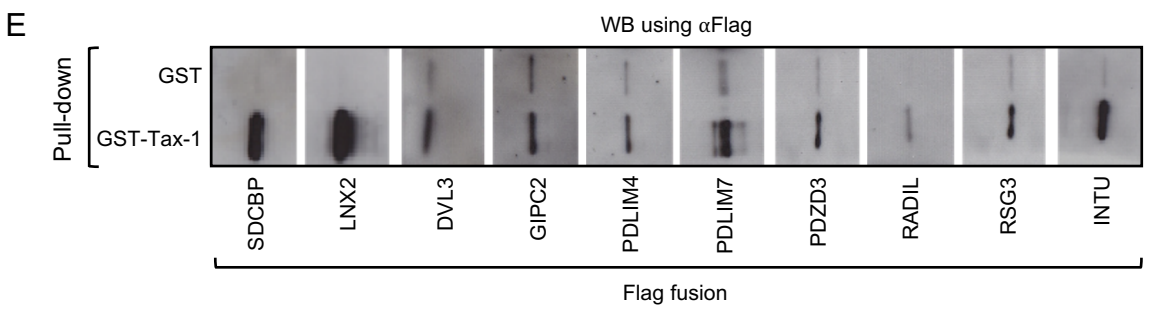

Figure S1. A comprehensive analysis of the Tax-1 interactome with human PDZ-containing proteins.
(A) PPIs between Tax-1 and human PDZ domain-containing proteins identified by yeast 2-hybrid (Y2H) and validated by GPCA, or using a pull-down assay (blue); and known PPIs from the literature (yellow). (B) Literature reported interactions between Tax-1 and human PDZ domain-containing proteins. (C) Heat maps of the Y2H assay by testing a library of 244 individualized PDZ domain-containing proteins fused to AD against DB-Tax-1. A growth score of “0”, “1” or “2” indicates a null, weak or strong interaction, respectively. (D) Representative Y2H assay plate lacking tryptophan (Trp), leucine (Leu), and histidine (His) where a growth score of “0”, “1” or “2” indicates a null, weak or strong interaction between DB-Tax-1 and PDZ-domain-containing proteins fused to AD, respectively. (E) Representative GST-pull-down analyses of proteins encoded by Flag-fused open reading frames (ORFs) available in the human ORFeome collection.

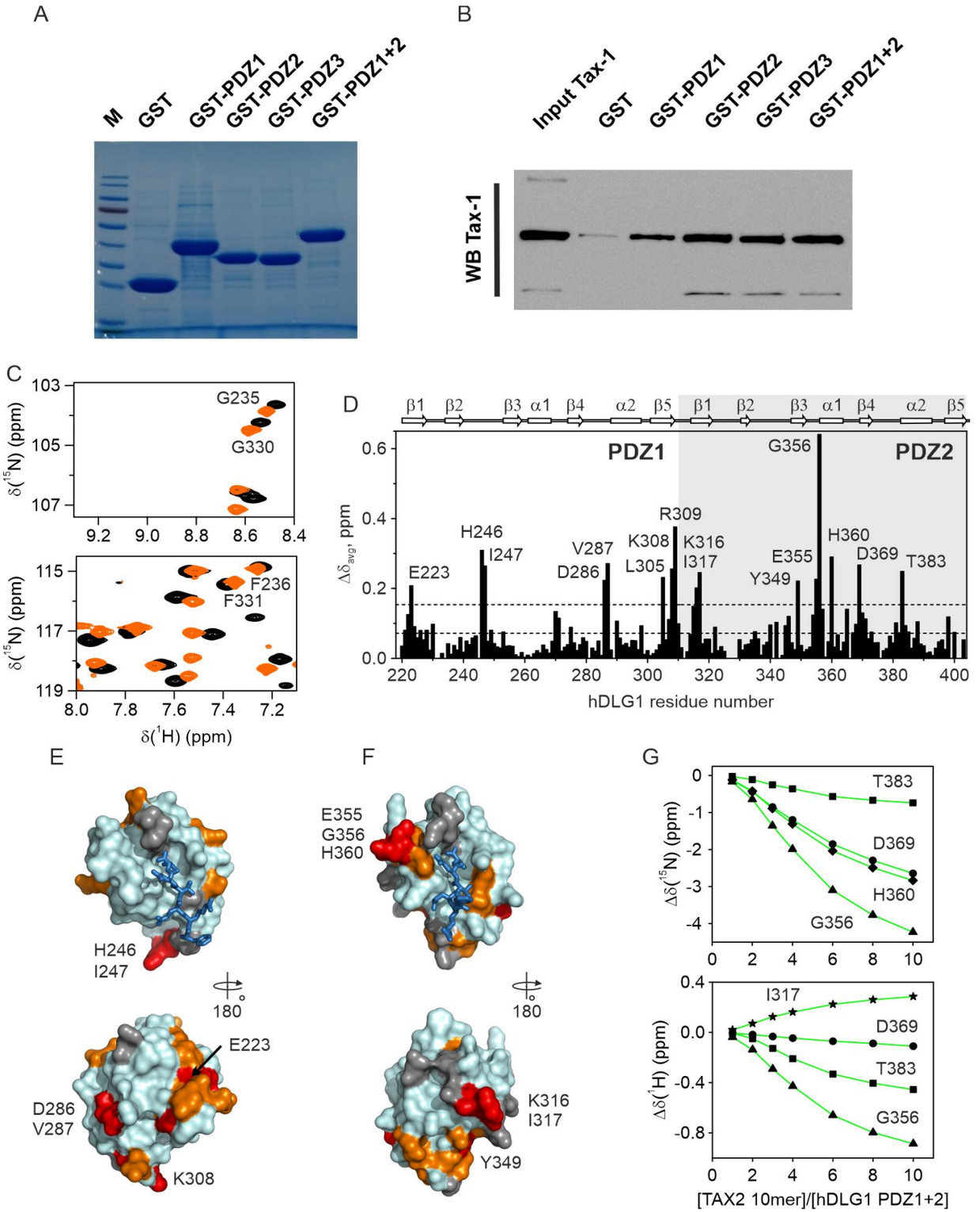

Figure S2. Validation of hDLG1 PDZ-Tax-1 interactions and NMR-observed binding of hDLG1 PDZ1+2 tandem to Tax 2.

(A) Purified GST-fused hDLG1 PDZ1 domains. (B) GST-pulldown assay using Tax-1 protein from HTLV-1 producing MT2 cells. (C) Overlay of selected regions of $^{1}H,^{15}N$ HSQC spectra in the absence and presence of Tax2 10mer (black and orange, respectively). The labels identify the backbone amide resonances affected by the Tax-1 10mer binding (cf. Figure 2. (D) $\Delta\delta_{avg}$ of the hDLG1 PDZ1+2 in the presence of 6 molar equivalents of Tax2 10mer. The horizontal lines show the average $\Delta\delta_{avg}$ and the avg + stdev. (E,F) Chemical shift mapping of the Tax2 10mer binding. The molecular surfaces of hDLG1 (E) PDZ1 and (F) PDZ2 domains are colored by the $\Delta\delta_{avg}$ values as in Figure 2C,D. The modeled C-terminal part of the Tax-1 peptide, bound to the canonical PDZ site, is shown in sticks as a reference. (G) Chemical shift perturbations ($\Delta\delta$) of the backbone N (left) and H (right) atoms for several hDLG1 PDZ1+2 residues indicated in the plots. The lines joining the symbols are only meant to guide the eye.

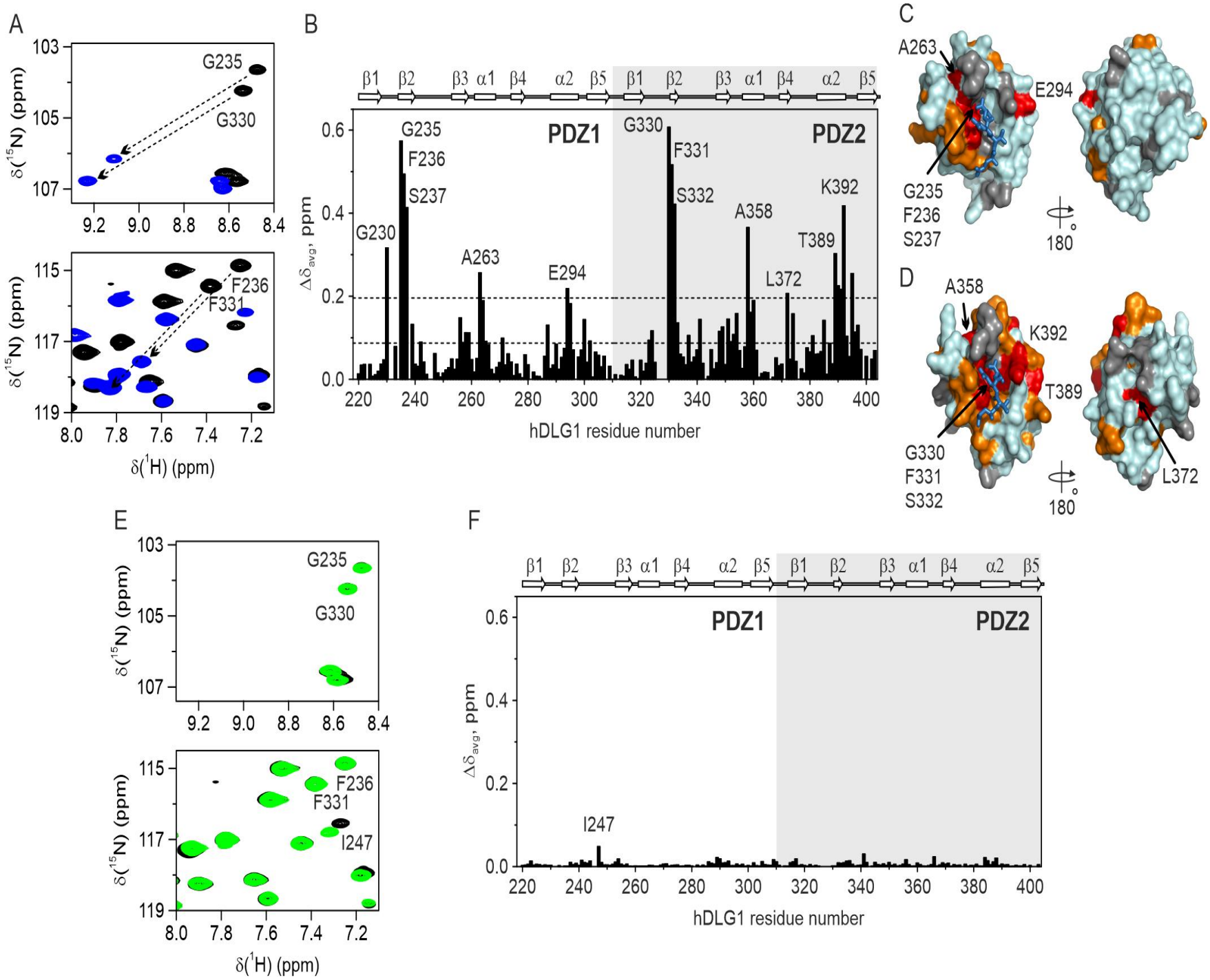

Figure S3. Control hDLG1 PDZ NMR experiments with Tax-1 PBM 4mer and N-terminal 6mer (6mer-N) peptides.
(A) Overlay of $^{1}H,^{15}N$ HSQC spectra of the free and PBM 4mer-bound ^{15}N hDLG1 PDZ1+2 tandem (in black and blue, respectively), with the chemical shift perturbations for the selected residues indicated by arrows. (B) $\Delta\delta_{avg}$ of the hDLG1 PDZ1+2 at saturating amounts of PBM 4mer. (C,D) Chemical shift mapping of the PBM 4mer binding. The molecular surfaces of hDLG1 (C) PDZ1 and (D) PDZ2 domains are colored as in Figure 2C,D. The modeled PBM peptide, bound to the canonical PDZ site, is shown in sticks. (E) The spectra of the ^{15}N hDLG1 PDZ1+2 tandem in the absence and presence of 6mer-N (black and green, respectively).(F) $\Delta\delta_{avg}$ of the hDLG1 PDZ1+2 in the presence of 6 molar equivalents of 6mer-N.The labels identify the sole residue with a significant binding shift.

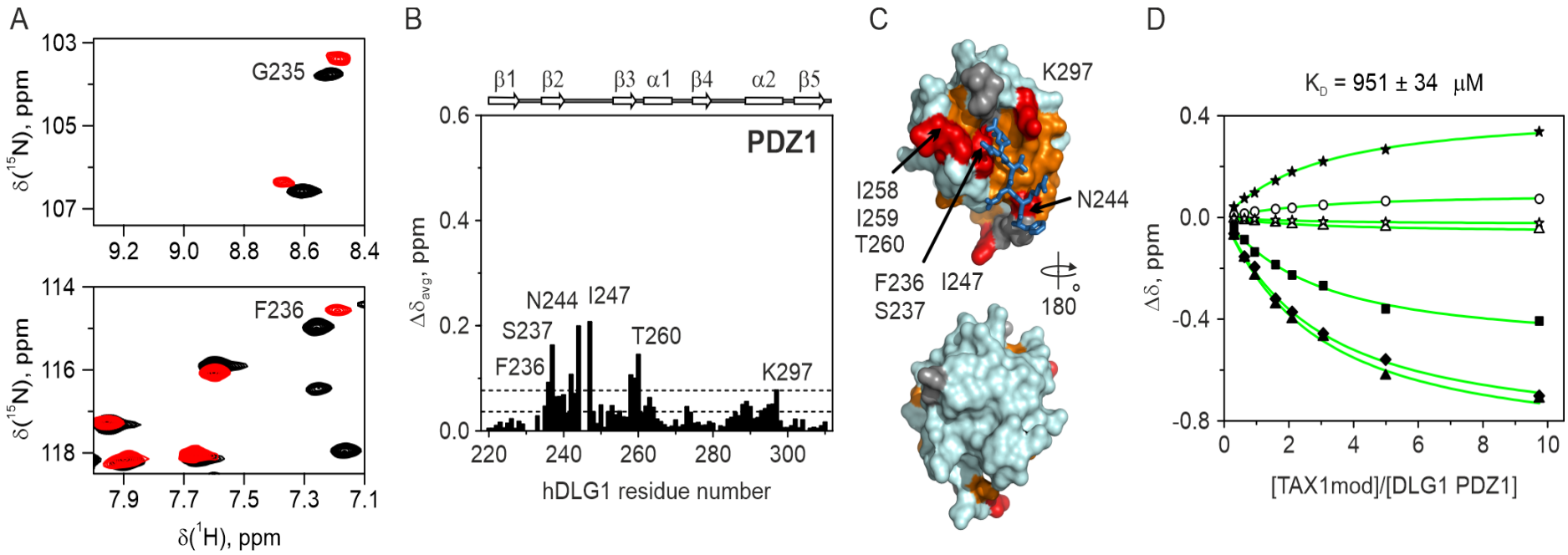

Figure S4. Control NMR experiments with the C-terminally amidated Tax-1 10mer peptide (Tax-1mod).

(A) Overlay of $^{1}H,^{15}N$ HSQC spectra of ^{15}N hDLG1 PDZ1 in the absence and presence of Tax-1mod peptide (black and red, respectively). The labels identify the backbone amide resonances affected by the Tax-1 10mer binding (cf. Figure 2E). (B) $\Delta\delta_{avg}$ of hDLG1 PDZ1 at saturating amounts of Tax-1mod. (C) Chemical shift mapping of the Tax-1mod binding. The molecular surface of hDLG1 PDZ1 is colored as in Figure 2G. The modeled C-terminal part of the Tax-1 peptide, bound to the canonical PDZ site, is shown in sticks. (D) NMR chemical shift titration of ^{15}N hDLG1 PDZ1 with the Tax-1mod peptide. Open and filled symbols refer to the chemical shift perturbations ($\Delta\delta$) of the backbone H and N atoms, respectively, of F236 (squares), G240 (circles), I258 (triangles), I259 (diamonds), and L296 (stars). The curves were fitted simultaneously to a binding model with the shared K_D (Equation 1). The solid lines show the best fits with the K_D value of 951 ± 34 μM.

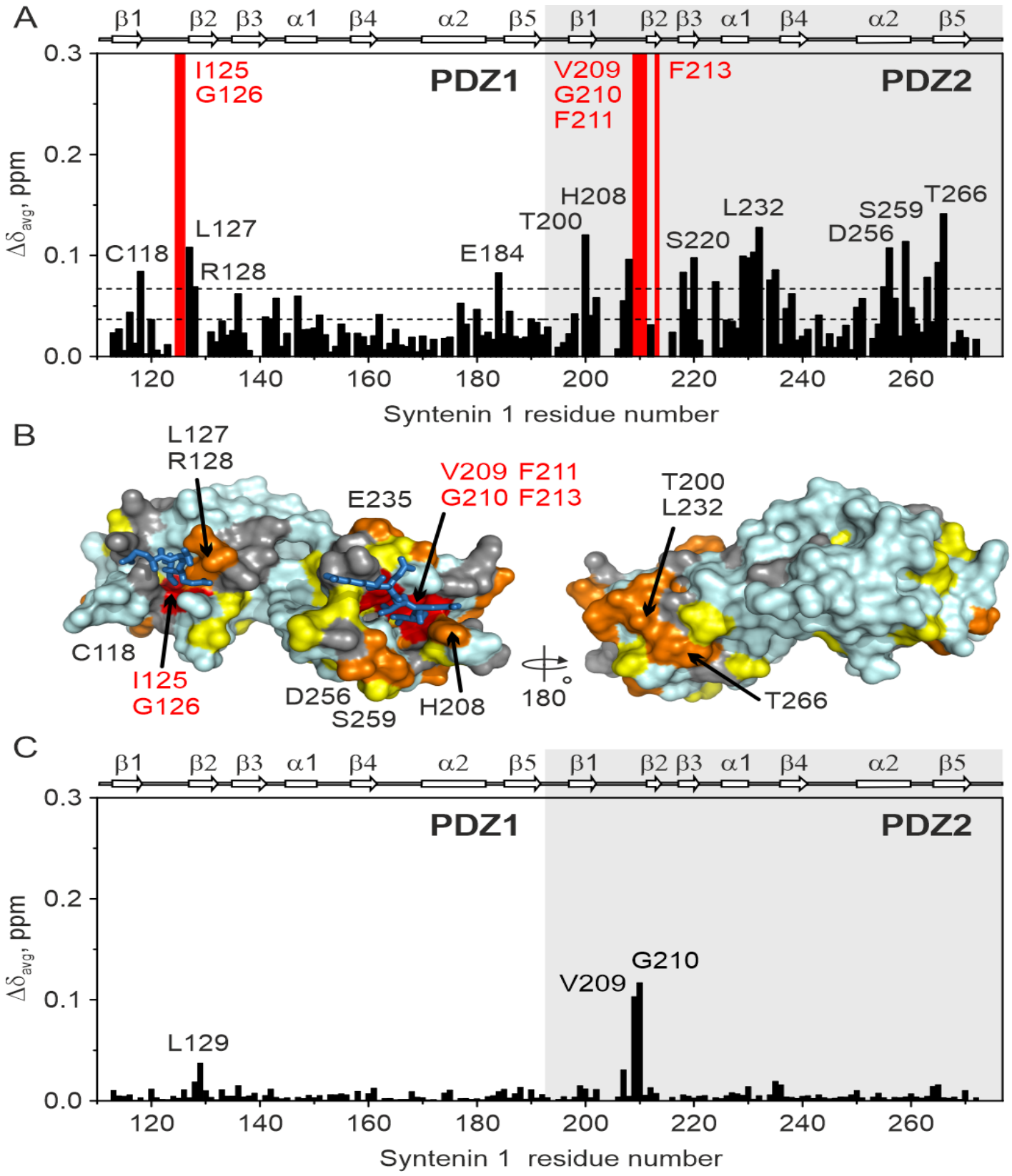

Figure S5. Control syntenin-1 NMR-experiments with Tax-1 PBM 4mer and 6mer-N peptides.
(A) $\Delta\delta_{avg}$ of ^{15}N syntenin-1 PDZ1+2 tandem in the presence of 6 molar equivalents of PBM 4mer. Residues with backbone amides broadened beyond the detection limit upon complex formation are indicated by red bars. (B) Chemical shift mapping of the PBM 4mer binding. The molecular surface of syntenin-1 PDZ1+2 tandem is colored as in Figure 4B. The modeled PBM peptides, bound to the canonical PDZ sites, are shown in sticks. (C) $\Delta\delta_{avg}$ of the ^{15}N syntenin-1 PDZ1+2 tandem in the presence of 7 molar equivalents of 6mer-N. Several residues with significant binding shifts are labelled.